AN INVESTIGATION OF STABILITY FOR A CLASS OF STEPPING MOTORS

A THESIS

Presented to

The Faculty of the Graduate Division

by

Edward Kevin Dahill

In Partial Fulfillment

of the Requirements for the Degree

Master of Science in Mechanical Engineering

Georgia Institute of Technology

June, 1971

In presenting the dissertation as a partial fulfillment of the requirements for an advanced degree from the Georgia Institute of Technology, I agree that the Library of the Institute shall make it available for inspection and circulation in accordance with its regulations governing materials of this type. I agree that permission to copy from, or to publish from, this dissertation may be granted by the professor under whose direction it was written, or, in his absence, by the Dean of the Graduate Division when such copying or publication is solely for scholarly purposes and does not involve potential financial gain. It is understood that any copying from, or publication of, this dissertation which involves potential financial gain will not be allowed without written permission.

7/25/68

AN INVESTIGATION OF STABILITY FOR A CLASS OF STEPPING MOTORS

Approved:

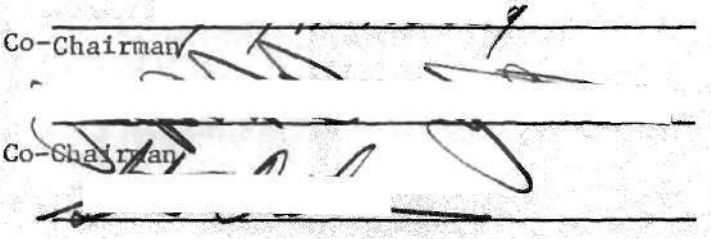

ACKNOWLEDGMENTS

The author expresses sincere appreciation and indebtedness to his thesis advisors Dr. Joseph R. Baumgarten and Dr. Jay H. Schlag, and to Dr. Stephen L. Dickerson. Their guidance and assistance were invaluable in the writing of this thesis.

Appreciation is also expressed to the National Aeronautics and Space Administration which provided the funds to permit the author to undertake study at the Georgia Institute of Technology, and to IMC Magnetics Corporation for technical assistance.

Special thanks are given to the friends and associates of the author whose unfailing confidence and fund of technical expertise were drawn upon heavily during the course of this investigation.

This thesis is dedicated to the author's parents whose encouragement and understanding made possible the completion of this thesis.

TABLE OF CONTENTS

Table of Contents Continued

LIST OF TABLES

LIST OF ILLUSTRATIONS

GLOSSARY OF ABBREVIATIONS

x_i	($i = 1, \ldots .?$) state variable describing parameter of system under discussion.
CF1	Coulomb friction acting on motor rotor.
CF2	Coulomb friction acting on the load.
VF1	Viscous friction acting on the rotor.
VF2	Viscous friction acting on the load.
u_1	Velocity of rotor divided by the magnitude of the same velocity.
u_2	Same as u_1 for load.
J	Rotor inertia.
J_1	Load inertia.
K	Spring rate.
τ	Torque
Res	Resistance of winding.
V	Voltage (also V_i)
i	Current (also i_j)
M_a	Mass, subscript indicates specific mass.
R_a	Radius, subscript indicates specific radius.
I_a	Inertia, subscript indicates specific inertia.
λ	Flux linkage.
w_n	Natural frequency.
w_d	Damped natural frequency.
l	Length
p	Mass density.
g	Acceleration due to gravity

Glossary of Abbreviations Continued

L	Inductance
W_a	Energy, subscript indicates system under study.
β	Damping ratio.
δ	Log decrement.
K.	Kilohms, refers to Figures only.
L.	Linearity, refers to Figures only.

SUMMARY

The instability of step motor systems is a current problem which impedes the use of these systems as direct digital to analog conversion devices. The major areas of interest for this investigation are experimental determination of the frequency bounds on stable regions of step motor and load exciation, and the use of digital solutions for descriptive differential equations, as a method of predicting instability of step motor systems. For the purpose of this study, instability is defined as the inability of the rotor to reverse stepping-direction without cogging. The motor used in this investigation was a fifteen degree step, variable reluctance motor.

The experimentation supported the programming goal by investigating the single step command and multiple step command response of twenty different flexibly coupled motor load systems. The response of these systems to single step command with regard to decay time and overshoot is presented. The frequency bounds for stable operations are defined experimentally and presented in conjunction with the digitally predicted bounds.

A general method of digitally predicting motor-load instability is suggested with appropriate FORTRAN programming documentation. This method is based on mathematically modeling of the motor and load response and on the determination of a pseudo-separatrix for the system. Results indicate that this method should predict system instability if the system is sufficiently well modeled.

CHAPTER I

INTRODUCTION

The step motor has been used since the early 1930's; however, the current emphasis on digital control has caused renewed interest in the application and theory of these direct Digital to Analog conversion devices. D/A conversion has remained a slow point of digital operations, while other aspects have increased in speed of execution. The step motor provides either a means of increased rate of D/A conversion, (with proper buffering) or a device for direct conversion from digital input to analog output.

A step motor also referred to variously as a stepper, a stepper motor, or a stepping motor produces a finite angular rotation whenever a pulse is input to the motor controller. There exist essentially two types of step motor, the solenoid ratchet type and the phase-pulsed synchronous type. The phase pulsed type, which is of interest here, is more complex theoretically, but easier to mechanize and presents greater long range potential. This type requires no dual assembly for reverse stepping as the ratchet type does, and it is standardized in sizes equivalent to the Bureau of Ordinance sizes for servo motors. The solenoid ratchet type is simpler theoretically; however it is difficult to tune in practical use and necessitates dual assembly for reversing rotation. A large number of failure modes also are present in this type; consequently it has lost many of its former proponents (1).

For the phase-pulsed type which was used in this study, there

are several types of stator phase excitation schemes possible. All types may be described in terms of the number of phases available and the number of phases active when the motor is being held stationary. For example, the three-phase motor normally has one phase active in the hold configuration, and the three-phase modified scheme utilizes two active phases in the hold configuration. In the first case the rotor poles align with the active stator poles, minimizing the magnetic flux; in the latter case the flux is minimized by centering the rotor poles between active stator poles. More active phases imply a higher holding torque; however, more complex control circuits and higher power use are required by these complex types.

The rotor may also be one of several types including permanent magnet, independently wire wound, variable reluctance, and combinations of these types, such as a wire wound permanent magnet type. Each of these types has its peculiar characteristics which may be desirable for specific design applications. The permanent magnet type for example requires no current input to hold a position. The magnetic field of the rotor acts to maintain the quiescent position without input power by minimizing the magnetic flux across the air gap.

Traditionally the step motor has been modeled by deriving a transfer function for the motor system. Kieburtz (2), Robinson (3), and O'Donahue (4) have presented linear and nonlinear approximations for classes of step motors. These empirical transfer functions are not based on the electromagnetic characteristics of the motors, but rather on the response exhibited by the motor system. More recently Chang (5) and Kuo (6) have published analyses which predict motor

response by means of electromagnetic theory. It is on the basis of this latter work that this study was conducted.

Stability

However the motor system is described, the question of most importance is that of stability for the motor-load at a given input pulse frequency. The command position for a step motor may be determined by multiplying the number of pulses (step commands) by the step size (increment) then adding this product to the initial angular position. Given the above, the essential stability criterion for step motor systems is straightforward. Does the motor-load system reach this command position in the required time?

This question may be subdivided into several distinct but related questions or criteria:

1) Does the motor-load system gain or lose a step while being driven by a pulse sequence?

2) Can the system initiate stepping upon command?

3) Is there excessive positional variation about the command position when no command pulses are being input?

4) Is there excessive motor or load velocity at any point in the transfer from one position to another?

5) Can the motor be stopped upon cessation of the driving pulse train and can it reverse stepping direction without loss of positional control or slowing down?

Of these questions, the third and the fifth are not germane to this investigation. It is assumed that proper mechanical or magnetic damping could be provided to alleviate the overshoot problem raised

by question three. Question five pertains to the slew or unidirectional region of motor operation. In this region, the step motor performs as an alternating current motor would perform. As successive phases are excited by the controller, the rotor slews past each command position. This region, while interesting, is not the primary region of operation for a step motor. The remaining questions form the basis for the investigation undertaken in this thesis.

Experimentally the parameters of interest were maximum stable step rate (input pulse frequency), system spring rate, and inertial load on the motor. Utilizing a three-phase, variable reluctance step motor (size 004), four inertial loads and five system spring rates were investigated. The system of load and motor was modeled by a digital computer utilizing a fourth order Runge-Kutta approximation to solve the system differential equations. On the basis of these solutions, the system response was predicted and compared to the experimental results by means of a digital plotting routine (the Calcomp plotter). The stability region was defined on the phase space of the motor by solving the system differential equations in reverse time. That is, t final and $\underline{x}$ final are utilized as initial conditions. As the integration proceeds, time (t) is reduced from t final to zero. (See Appendix I.) This procedure yields a separatrix which can be compared, by the computer, to the state variables describing motor position in order to determine stability for a given frequency of pulse input. The results are not conclusive, but this approach apparently yields a method of predicting stability for the systems investigated.

CHAPTER II

INSTRUMENTATION AND EQUIPMENT

The primary piece of experimental apparatus for this investigation was the step motor and its controller-driver. All other apparatus was used either to support the motor and load, to provide power to run the motor and controller, or to detect the positional variation accompanying step response. Table 1 is a complete list of the equipment and instrumentation used. However, it is somewhat misleading since not all the items listed in the table were utilized concurrently. Concurrently the usage of many items is obvious.

The motor, bearings, and the linear potentiometer were positioned on the base plate using three sixteenths inch aluminum angle, which had been reamed to act as mounts. The diameters and specifications for these mounts are listed in Table 2. These mounts functioned as rigid support for the equipment and provided for alignment of the motor and load system. Throughout the experimentation, power was provided for the motor by the 50 volt (D.C.) source listed. This voltage was supplied to the controller-driver following the IMC Magnetics specifications for that driver (see Figure 1). The function generator was used as a source of pulses for the controller-driver. The direct current offset in this device permitted the production of a positive pulse of 15 v.d.c. amplitude without external clipping circuits. This was the amplitude required by the controller-driver for successful operation.

Table 1. Instrumentation and Equipment List

15 degree step motor	IMC Magnetics 020-004 VR
Selenium photocell	Tandy Corp. 276-115
Step motor controller driver	IMC 0128-15-3312-01
Function generator	Hewlet-Packard 3310A
Magnetic velocity transducer	Bruel and Kjaer Type MM002
Dual beam oscilloscope	Tektronix Type 502A
D.C. power source	Sorensen Nobatron T50-15 %0 VDC max.
D.C. battery 3 volt	Eveready W356
Potentiometer 10K 1 turn	Helipot Model 5433 5% Linearity
Potentiometer 40K 10 turn (2)	Helipot 7223-15 L .075%
Beam balance	O'Haus Triple Beam
60 tooth worm wheel pitch diam. .9375, 3/16 ID*	PIC Corporation
Worm pitch diam. .5, 3/16 ID	PIC Corporation
Couplings 1/4 ID (4)	Boston Gear Co.
Roller bearings 1/4 ID (2)	S-K Corporation
3/16 aluminum angle	Machined to specifications of Table 2
Reduction shafts (assorted lengths)	1/4 to 3/16
.045 diameter steel wire	Cut to spring size
Experimental baseplate	PIC Corporation
Oscilloscope camera	Polaroid Corporation
Light source and power for source	Machined or experiment Heathkit 12 volt source

Table 1 Continued

Brass slug 1/4 ID	Machined for experiment**
Aluminum slug 1/4 ID	Machined for experiment**
Assorted 1/4 OD Shafts	Centerless ground
Approximately 5 feet shielded cable	
Assorted PIC Corporation fittings for support of worm, and measurement of angular rotation.	

* All dimensions not indicated are in inches.

** See Appendix III for specifications and derivation of Inertia for slugs used.

Table 2. Mount Dimensions

Bearing Mounts (2)	
Centerline height	1.75 inch
Hole diameter	.75
Face dimensions	3. x 2.
Potentiometer Mount (1)	
Centerline height	1.75
Hole diameter	1.325
Face dimensions	3. x 2.5
Motor Mount (1)	
Centerline height	1.75
Hole diameter	1.75
Face dimensions	3. x 3.

Potentiometer and motor were mounted using three mounting clamps at 120^{o} angles around the hole circumference. The bearings were press fit.

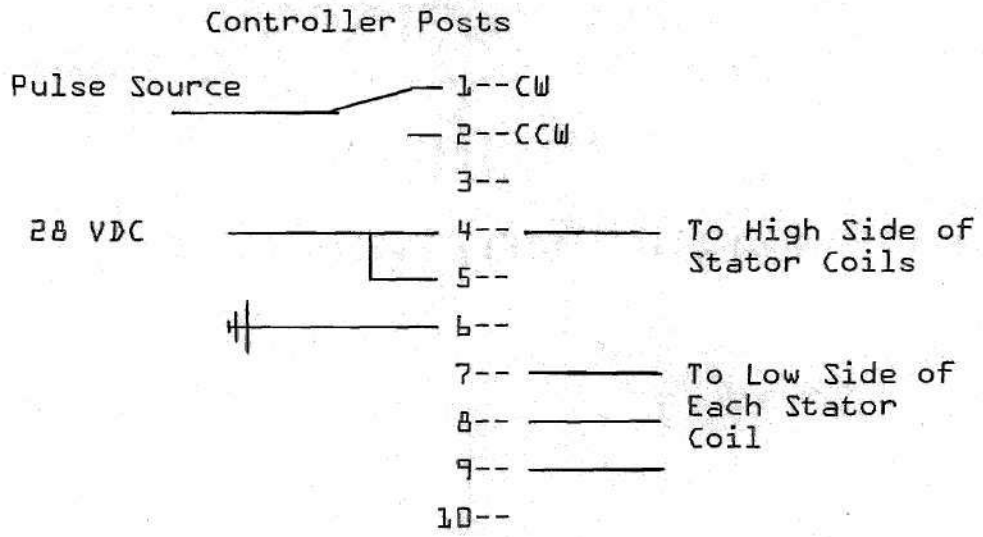

Figure 1. Motor Controller Wiring

Brass Fittings -- Steel Spring
Distance Between Mounts Variable

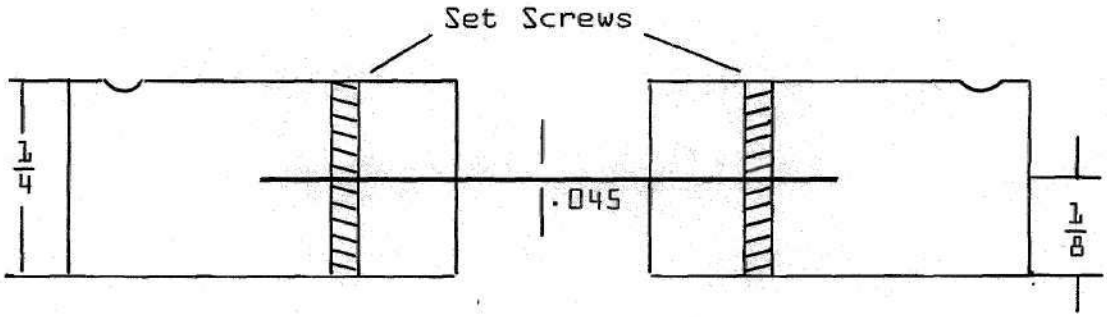

Figure 2. Spring Mounts

The oscilloscope and camera detailed were also used throughout the experiment for recording the output of the test instrumentation. All results of significance were recorded (photographed) for later study and analysis utilizing Polaroid film. This permitted reference and accuracy of measurement obtainable by no other means. Photographs were inspected with a three power magnification provided by a standard philatelist's glass.

In order to provide a standard repeatable spring rate for the experimental motor-load system, the apparatus illustrated in Figure 2 was used. Essentially it consisted of a pair of wire grips which could be held easily by the standard one quarter inch coupling used. This arrangement provided for localized spring rate in the system which could be defined analytically. The dual set screws were both a machining convenience and permitted positioning of the wire within the mounts and provided for adequate holding torque. The dimple on the rear of the mount prevented excessive scoring of the mount by the set screws of the couplings used. The avoidance of scoring facilitated change from one system of springs to another. Wire, forty-five thousandths in diameter, provided the springs for the systems investigated. The wire was cut so that when the ends were touching the bottom of the mount center holes, the separation between the mount set screws was either one, two, three, or four inches. Repeatability for the various inertias was then obtainable. The load inertias were supplied by the slugs mentioned in Table 1 and by the steel shaft used to support them. At this point, the instrumentation must be separated into two categories, that used for detection of single

step response, and that used for multistep response detection.

Single step response may be defined as the response of the motor and load to a single input pulse. In this case, the step was a fifteen degree step from the stopped configuration. The photocell was used for detection of single step response of the system. The cell itself was mounted on an insulated backing material (plexiglass) and wired into the circuit shown in Figure 3, using shielded cable throughout (it was found helpful to shield the photocell leads also). The photocell was not masked on the surface of the cell (see Appendix II) although this method has had some success. Rather masking was provided by a shutter fixed to the shaft of the motor. As the shaft rotated through 15 degrees and oscillated about the command position, the shutter (mask) also oscillated changing the amount of light striking the photocell causing voltage fluctuation sensed by the oscilloscope. The shutter finally used was a paper, cardboard laminate with forty-five thousandths wire reenforcement shown schematically in Figure 4. This provided sufficient rigidity while minimizing the loading of the motor load system. For the unloaded motor investigation, the shutter was fixed to the motor shaft. For testing the load assemblies, it was fixed to the load shaft. In both cases bonding was accomplished by use of cement. In the latter case, the spring assembly was mounted between the motor and the load shafts. The overall assembly is shown in an overhead schematic in Figure 5.

Although it was not used for detection of the single step response, the linear potentiometer for multistep sensing is included

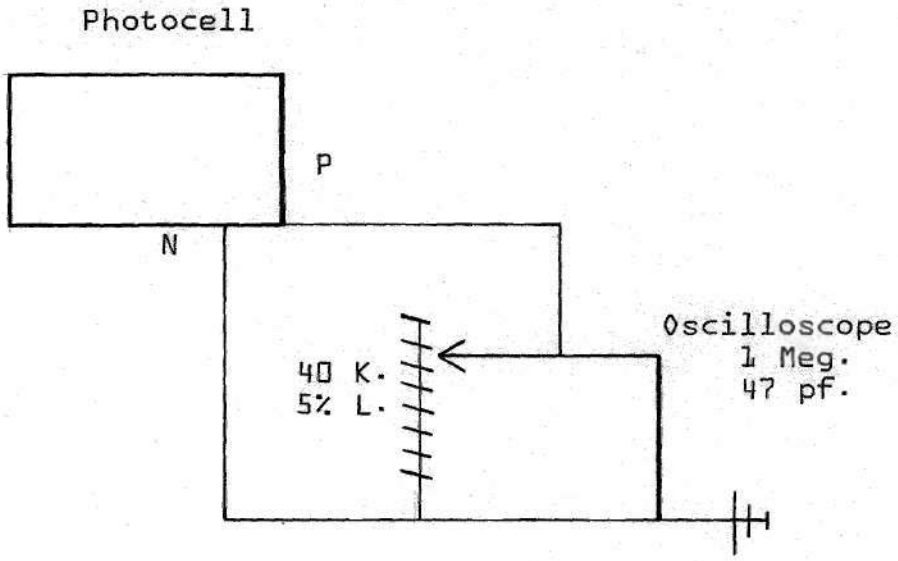

Figure 3. Photocell Circuitry

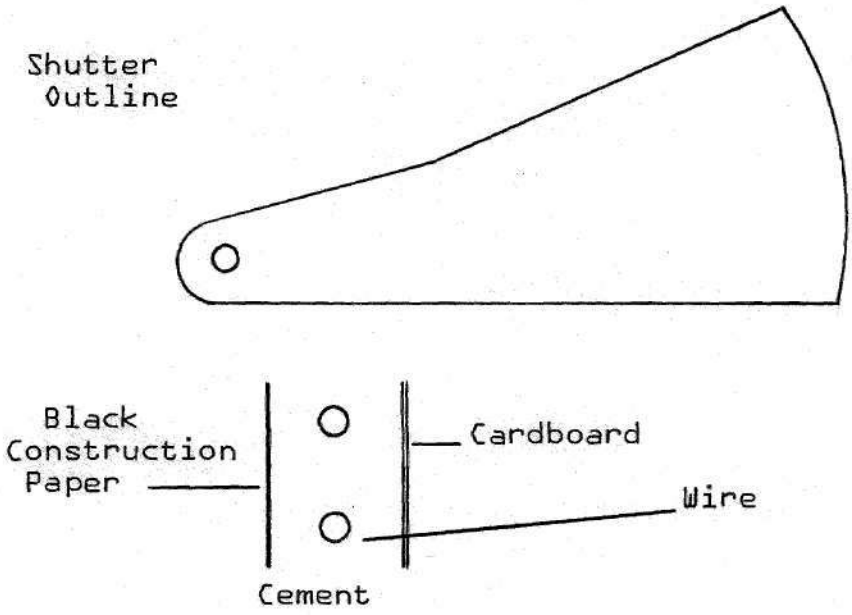

Figure 4. Shutter Construction with Lamination

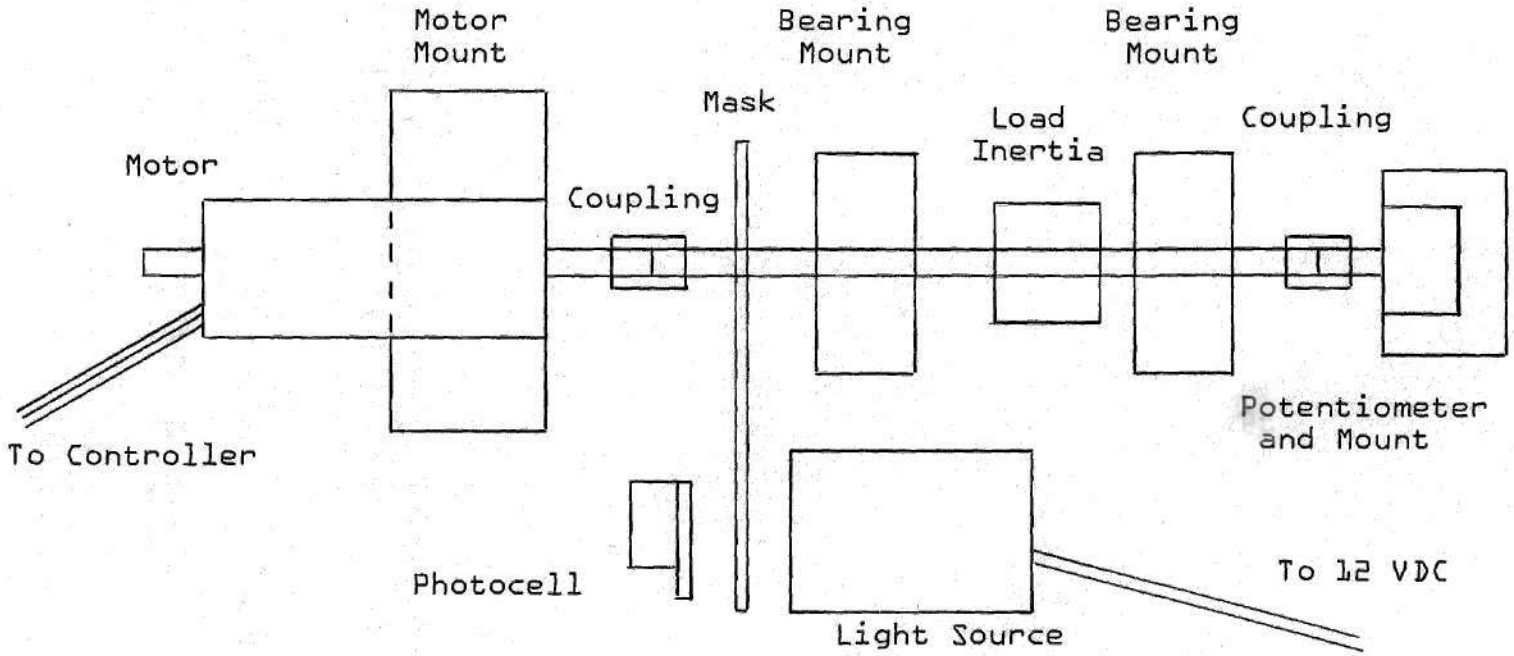

Figure 5. Schematic Overhead View of Single Step Assembly

in Figure 5 since the friction and slight additional inertia of the potentiometer shaft were present in the experimentation on loaded motor systems. The potentiometer was rigidly connected to the load shaft using the standard one quarter inch I.D. coupling. The potentiometer was wired into the adjusting circuit shown in Figure 6. The instrument used did not have stops at either end of the single turn; thus it permitted continuous rotation without concern for potentiometer damage. In sensing the multistep response, the dual trace facility of the oscilloscope was used. This permitted monitoring of both the potentiometer output and the output of the function generator (pulse frequency).

The magnetic transducer was mounted perpendicular to the motor shaft. A high permitivity disk was mounted on the shaft to act as a wobble plate for the transducer face. The transducer, which is velocity sensitive, detected the variation in the air gap as the shaft rotated through 15 degrees. The high permitivity disk was fixed to the shaft with a water soluble cement. A schematic is shown in Figure 7 indicating the relative positions of the motor shaft and the transducer.

Different calibration techniques for the two investigations were also required. The multistep testing was calibrated using the circuit indicated in Figure 6 to provide voltage adjustment. The calibration of the photocell was somewhat more difficult. A 60 tooth worm wheel was attached to the motor shaft by means of a reduction shaft and the standard coupling. The worm itself was mounted (on standard PIC Corporation bearings and hangers) perpendicular to the

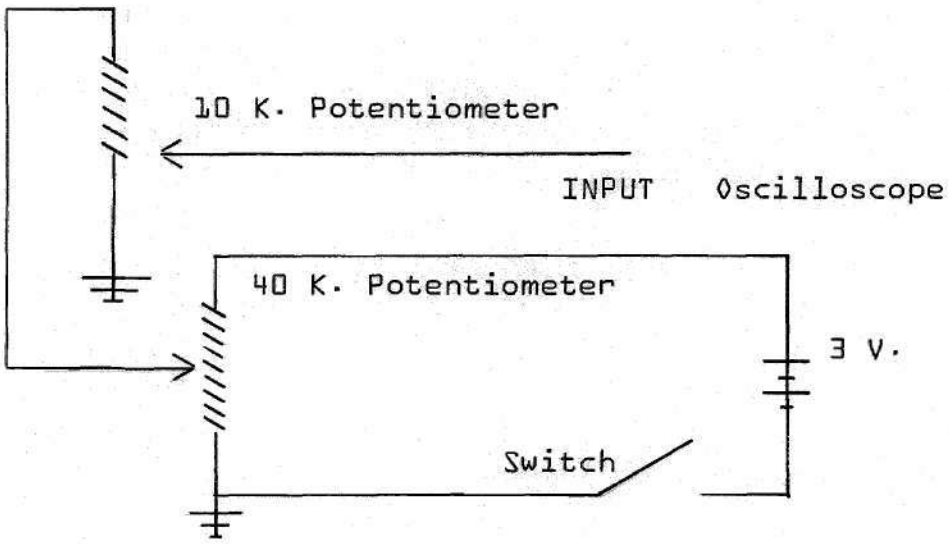

Figure 6. Multistep Sensing Circuitry

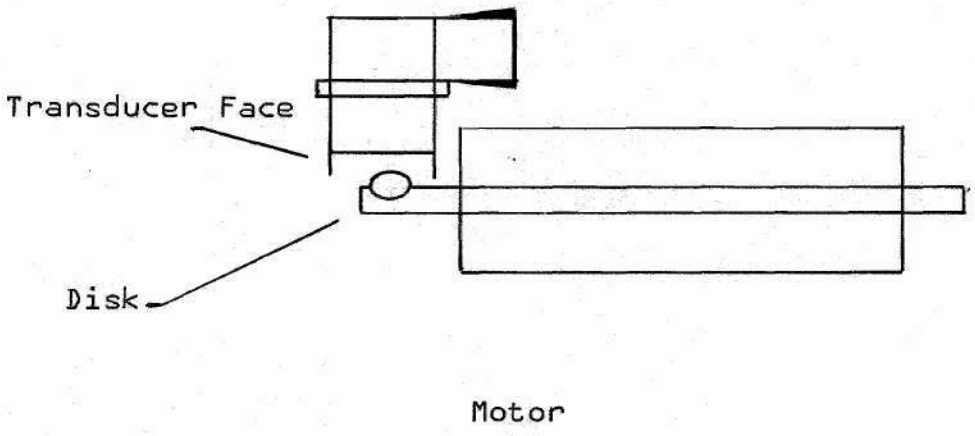

Figure 7. Velocity Transducer Schematic

motor shaft. Rotation of the worm resulted in shutter rotation. Passing between the light source and the photocell, the shutter caused voltage reduction as the lighted surface area was decreased. A 360 degree rotation of the worm resulted in a six degree rotation of the motor shaft. The amount of angular rotation was described by mounting a standard 360 degree wheel on the worm shaft, with an independently mounted indicator mark.

The remaining instrumentation or equipment used was a digital computer, in this case a FORTRAN programmable Univac 1108. This device was used to predict the response of the motor by means of a Runge-Kutta approximation; the programming details will be discussed in Chapter IV.

CHAPTER III

EXPERIMENTAL PROCEDURE

The procedures followed in pursuing this investigation are best discussed after a preliminary division into two major divisions and several minor subsections for each division. This chapter is devoted to the first major topic, physical experimentation. This topic is most clearly presented by reviewing three subdivisions: preliminary investigations, single step system response, and multiple step system response. Although the two major areas of study were pursued concurrently, the physical experimentation shall be discussed prior to the digital investigation which is reserved for the following chapter.

As noted in the preface to this chapter, the physical investigation will be discussed in segments. Many procedures are common to several segments, and as such, will not be discussed more than once. These common areas are fairly obvious and will be denoted only when they recur in later discussions. Several procedures which are standard operations were also used; these shall not be discussed in detail, but shall be noted as standard whenever they arise.

Preliminary Investigation

The preliminary investigation was concerned with determination of the motor parameters for the purpose of later digitally modelling the motor as an independent device. There were several parameters which needed definition for the particular motor under study.

The coils of the motor stator were pulsed with a voltage of 20 volts. The motor was locked in two distinct configurations for this pulse testing by the rotation of the worm wheel discussed below. The rotor was first locked in the aligned position; that is the rotor and stator poles were aligned. This position was determined by freeing the worm wheel and pulsing the motor into a hold configuration. A pulse was then applied and the resulting voltage response of the single stator phase was recorded on polaroid film. The rotor was then rotated 22.5 degrees so that it was in an unstable node condition. That is the rotor teeth were between two active stator poles. This positioning was checked by observing that at this point, the rotor received zero net torque although a stator phase was energized. After locking the worm wheel, the energized phase was de-energized and then pulsed as described previously. This resulted in photographs of the response for the maximum and minimum inductance positions of the rotor. By performing standard calculations on the RL time constant observed, the inductance could be calculated (see Appendix IV). The resistance of each stator phase was checked with a standard ohmeter and conformed to the manufacturer's specification of 20 ohms. This data was used as noted above to determine the electromagnetic characteristics of the motor.

Although the determination of the mechanical characteristics of the motor was completed in the single step response investigation, it is appropriate to discuss what became a standard procedure at this point. The static friction or stiction was evaluated by wrapping 14 pound test monofilament around the motor (later the load) shaft and

loading the monafilament until motion due to gravity occurred. A mass or weight table was constructed of plywood with a hook for suspension from the monofilament. This facilitated the loading process and permitted rapid measurement of the required load. In every case, the maximum possible stiction was recorded. If bearings of misalignment caused a higher loading at one point of the full rotation, it was this figure which was recorded. The standard shaft diameter for this test was one quarter inch, and the load was measured on a mass balance under a conversion of 453.6 grams/pound force. These mass measurements were later used in the digital programming detailed in Chapter IV. The remainder of the motor mechanical parameters were determined under the conditions of response to a single step command as described below.

Single Step Response

The single step response of the motor alone and of the motor when flexibly coupled to a load was investigated using a photocell position transducer. The transducer consisted of a 500 millivot, 600 microampere photocell, as specified in Chapter II, with dimensions one and one eighth inches, yielding a sensitive area of one and eight hundred seventy-five thousandths inches squared. The cell was mounted on an insulated backing of plexiglass and adjustment slots were provided for lateral and longitudinal positioning. The cell was illuminated by a 14 volt bulb of the auto clearance light type with power supplied by a 0 to 15 volt (adjustable) Heathkit power source. The light fixture used was a standard bulb socket inserted in a foil lined tube of construction paper. This provided focusing for the

light source. A uniform distribution was obtained by masking the open tube end with two layers of vellum. This procedure generated a uniform intensity pattern of light which illuminated the surface of the photocell. The photocell and the light source were bolted to the PIC experimental base using standard 1/8 inch mounting nuts and bolts. The mask or shutter mentioned in Chapter II was fixed, initially to the motor shaft, and later to the load shaft with cement.

Testing of the photocell was performed by mounting a worm wheel on the motor shaft and mounting the worm itself perpendicular to the shaft on standard 3/16 inch bearing mounts. The cell output was sensed by an oscilloscope equipped with a polaroid camera attachment, at a sensitivity of 20 millivolts per centimeter. Rotation of the worm shaft caused a reduced rotation of the motor shaft. The gear ratio used resulted in a six degree rotation of the motor shaft for every 360 degree rotation of the worm shaft. By freeing the worm wheel and exciting one phase of the motor stator, a zero point was established. Relocking the worm wheel, at the established zero point, the test procedure was initiated. The zero was recorded by a single trace on the polaroid film. Successive worm rotations of 180 degrees yielded a linearization pattern photographed in three degree increments of the motor (or load) shaft rotation. This pattern or linearization curve was photographically recorded for each system subjected to single step excitation. Initially an attempt was made to obtain a linearization over the entire range of rotation. However this was impossible due to the large angular overshoot exhibited by some of the systems tested. The sample linearization of Figure 8 shows that fairly good linearization

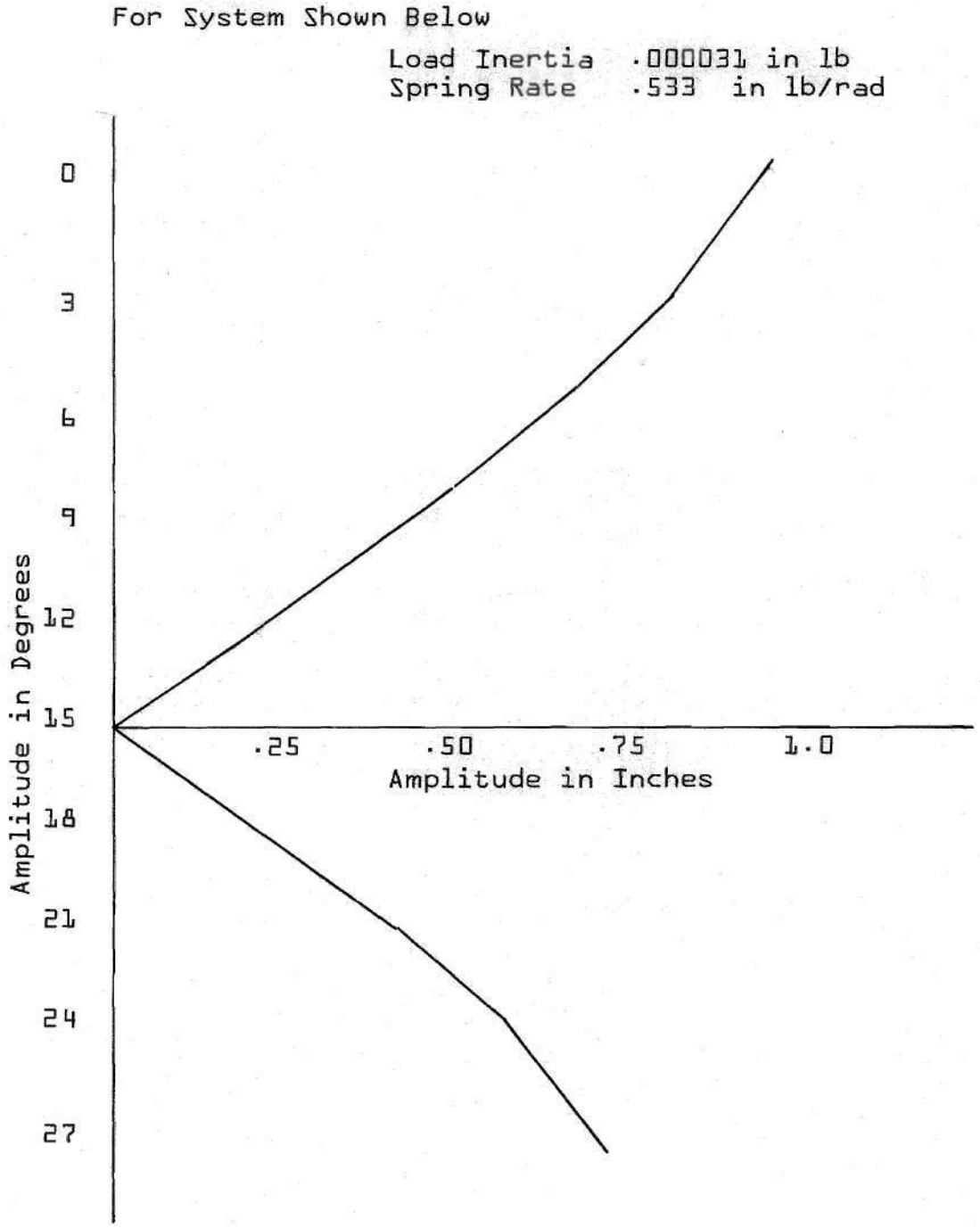

Figure 8. Sample Linearization of Photocell Transducer

was obtained by adjusting light intensity (voltage and current to the bulb), cell to light source distance, shutter placement and the angular relationship between the photocell and the shutter (approximately zero degrees at line between the center of the shaft and the centerline of the photocell).

Several shutters were examined before the paper laminate detailed in Figure 4 was decided upon. Initially it was problematic whether the shutter loading on the shaft during the actual testing was significant. Also the question of possible slip between the motor (load) shaft and the shutter was open. The calculations of Appendix III demonstrate that shaft loading of the first tested aluminum shutter was significant. This was minimized by the paper and wire shutter. However, the laminate shutter was less rigid and was possibly subject to lateral wobble (between the photocell and the light source) and vertical flexing under acceleration. In order to investigate these consequences of the lighter shutter, a secondary method of sensing the shaft vibration was necessary. The B and K velocity probe specified in Table 1 is a velocity sensitive vibration detection device. It detects vibration as a function of the varying reluctance of an air gap. Cementing a high permeability disk to the motor shaft, an air gap appropriate for vibration detection was created when the probe was mounted perpendicular to the shaft. By stepping the motor once and recording the vibration by photographing the transducer (probe) output on an oscilloscope, a source of comparison data was provided. These probe results were used to indicate the proper shutter selection and cementing procedure. In the motor test, water soluble cement was

used, testing as above indicated no slip. Later when the shutter was load shaft mounted, permanent epoxy was used. In both cases the velocity probe was used for comparison purposes.

Twenty different load, spring rate systems were tested in the single step and multiple step modes. These are detailed in Tables 3 and 4 and in Appendix III. For each system the characteristics of the photocell were recorded as above. Then the single step response was photographically recorded for each system. The twenty systems were mounted and tested independently; however, all systems with the same load inertia were tested consecutively. The procedure for testing the stiction was not applied to every case of the single step response. It was applied to at least two of the five spring rates tested for each inertial load. The testing of the single step response began in the hold configuration. The succeeding stator phase was energized while simultaneously de-energizing the currently active phase. The controller driver accomplished this switching when subjected to an input command. The resulting fifteen degree step was observed using the previously detailed photocell position transducer. The results were recorded photographically for later study for each load and spring system. In several cases, due to the high overshoot observed, two photographs were necessary to record accurately the overshoot which the system displayed. Thus photographs were taken for two successive steps, implicitly assuming that the steps were symmetrical. This procedure was justified in the data reduction which followed the experimentation.

The photographs of each system response were examined under a three power lens. The amplitudes of the overshoot and undershoot were

Table 3. Single-Step Loading

Spring Rate in lb/rad	Shaft Load in $lbx10^{-5}$ sec^2	Shutter Load in $lbx10^{-5}$ sec^2	Mount & Coupling Load in $lbx10^{-5}$ sec^2	Total Load in $lbx10^{-5}$ sec^2	Stiction in $lbx10^{-3}$
00	0.0	.91224	0.0	0.0	4.16115
00	.1331	1.16878	.712	27.838	46.131
.533	.1387	"	.307	27.091	18.711
1.066	"	"	"	"	"
2.133	"	"	"	"	"
4.267	"	"	"	"	"
00	.1331	1.6878	.712	25.472	43.182
.533	.1387	"	.307	24.720	15.432
1.066	"	"	"	"	"
2.133	"	"	"	"	"
4.267	"	"	"	"	"
0					
00	.1331	1.6878	.712	5.5423	39.145
.533	.1387	"	.307	4.7910	21.385
1.066	"	"	"	"	21.192
2.133	"	"	"	"	25.876
4.267	"	"	"	"	34.97
00	.1331	1.6878	.712	3.1773	44.147
.533	.1387	"	.307	2.425	17.8847
1.066	"	"	"	"	"
2.133	"	"	"	"	"
4.267	"	"	"	"	"

Table 4. Multiple-Step Loading

Spring Rate in lb/rad	Load Inertia in lb sec^2 x 10^{-5}	Motor Inertia in lb sec^2 x 10^{-5}	Stiction in lb x 10^{-3}
00	0.0	1.49524	39.242
.533	.71274	1.60196	32.518
1.066	"	"	"
2.133	"	"	31.360
4.267	"	"	31.388
00	0.0	3.8556	46.214
.533	3.1088	1.60196	37.202
1.066	"	"	37.092
2.133	"	"	40.619
4.267	"	"	32.628
00	0.0	23.7845	36.017
.533	23.0377	1.60196	37.313
1.066	"	"	41.667
2.133	"	"	39.131
4.267	"	"	37.037
00	0.0	26.15054	37.010
.533	25.4037	1.60196	36.0588
1.066	"	"	25.546
2.133	"	"	24.746
4.267	"	"	27.916

recorded in inches and translated by means of the linearization curves into degrees of angular rotation. In cases where two photographs were required, due to the complete masking of the photocell at the extreme, the amplitudes observed were recorded and compared to oscillations which were completely defined on a single photograph. Thus initial overshoot data was obtained from one picture, and successive values from another. The comparison of the amplitudes of oscillations which were completely visible on both photographs of the system response justified the assumption of equivalence (see Figure 9).

The photographic results were reduced to a set of data points suitable for digital manipulation by recording the amplitudes, and the time from step command for the maxima, and the times when the response trajectory equalled fifteen degrees (.262 radians). These experimental curves (points) of Appendix V were plotted by the Cal-Comp-Plotter routine of the Univac 1108 system at the Georgia Institute of Technology from the data points obtained as explained above. These experimental points also determined the system damped natural frequency and the log decrement for the system.(see Appendix VII). These parameters were used in modelling the single and multiple step response of the system and will be further discussed in Chapter IV under the digital modelling section.

Throughout the data reduction no steady state error was measured, although it is quite apparent that it should theoretically be present. This is due to the method of data reduction. The amplitudes of overshoot and undershoot were measured from the fifteen degree quiescent line. Since the motor was stepped into hold position prior

Step 2

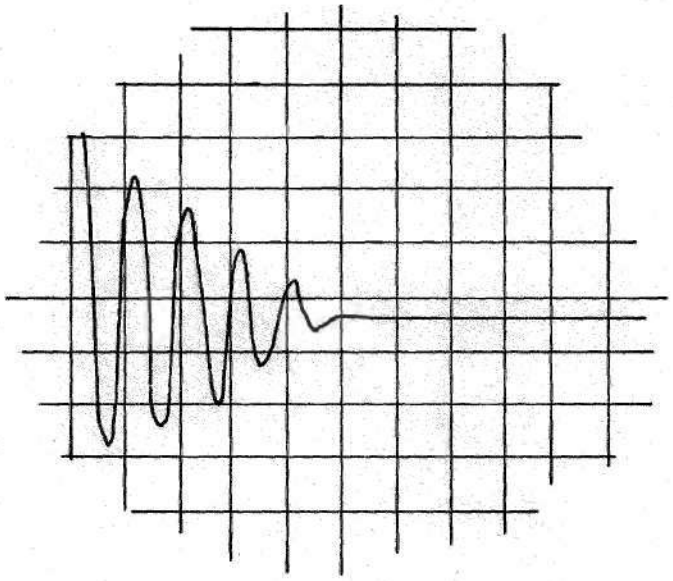

20 mv/cm 50 ms/cm

Step 1

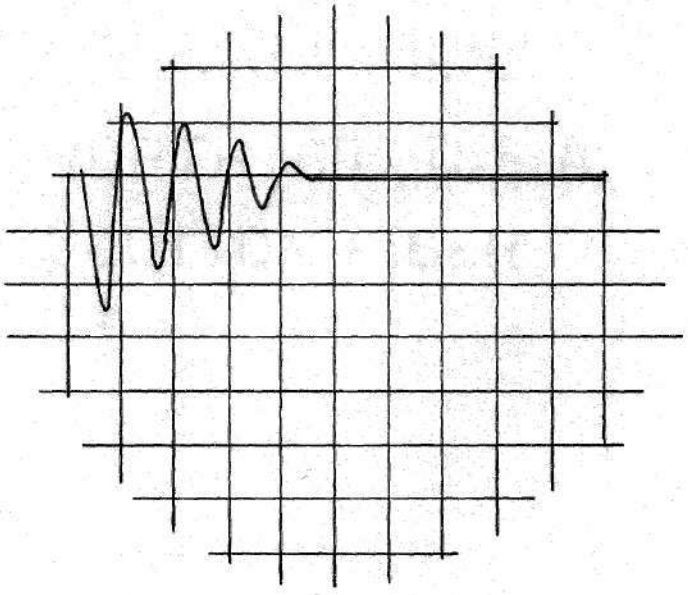

Load Inertia .000031 in lb

Spring Rate .533 in lb/radian

Figure 9. Sample Phototransducer Output
Single Step

to the step response observed, it is assumed that any error in angular position is consistently present for each step. This thinking also applies to the constant lag angle necessary for the production of load moving torque.

Multiple Step Response

The multiple step investigation closely resembled the single step investigation in the use of load inertias. The load systems investigated were in fact identical to those used in the single step investigation except for the reduction due to removal of the shutter (mask). The systems used in this segment of the study are listed in Table 4. As in the single step investigation, the various spring rates for a particular inertia were studied sequentially. In every case, the stiction was measured and recorded by the procedure previously detailed. However, the investigation of the multistep response utilized different sensing devices and required the introduction of a qualitative criterion for stability definition.

The sensing of the multistep response was accomplished by direct rigid coupling of the load and a single turn 10 Kilohm potentiometer. The potentiometer had no stops and was included in the measurements of the single step response in order to take into account the inertia and particularly the additional damping friction due to the slider of the potentiometer. The bias circuit was detailed in Chapter II and needs no further description.

The criterion for stability determination is straightforward both theoretically and experimentally. Can the motor reverse switch-

ing direction without cogging or losing step? Experimentally this was investigated by reversing a single poll single throw switch wired between the controller driver posts one and two (see Figure 1), while the driver was excited by the function generator. The frequency of the pulse input was increased until instability was apparent (due to obvious cogging). Subsequently the pulse frequency was reduced until a stable frequency was observed. At this stable frequency the motor could switch without cogging although in some cases excessive load positional variation occurred. The frequency was then increased until, by hunting, a maximum stable frequency was established for the stable region under study. There is an element of experimental judgement involved here since the complex nonlinear nature of the system made definition of a single maximum stable frequency for any region impossible. Observation of the potentiometer output for each frequency examined enabled definition of stability limits by comparing the system oscillation to the pulse output of the function generator which was also displayed. In regions near the stability limit, the coincidence of oscillation maxima and pulse input indicated the presence of a limit. These maximum stable frequencies were recorded photographically for comparison to the analytically predicted limits. After obtaining a photograph of the first maximum stable frequency, a second and in some cases a third upper frequency limit for the succeeding stability regions was sought and identified by the same procedure (see Figure 10). In each case a stable region was defined somewhat simplistically as a pulse frequency region within which the motor could reverse as defined above. In

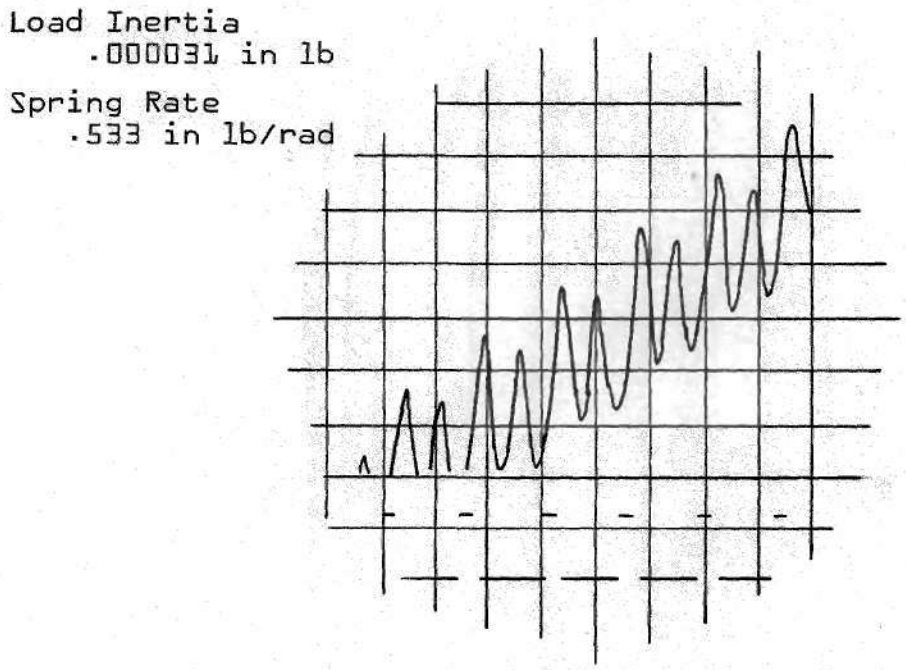

Figure 10. Sample Potentiometer Output Multistep Response

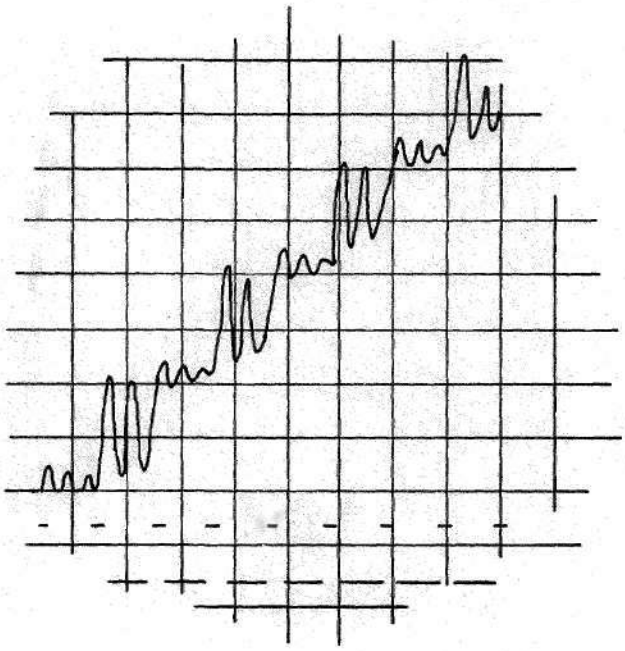

Figure 11. Noncritical Frequency Response

some cases, unusual system response was recorded for future comparison to the digitally predicted response (see Figure 11). The determination of the stable frequency regions for the various load systems concluded the experimental investigation.

CHAPTER IV

DIGITAL PROGRAMMING INVESTIGATION

This chapter is devoted to the discussion of three interrelated subareas of the digital programming investigation; modeling of system response, determination of a pseudo-separatrix for the system, and inquiring into the stability region (stable excitation frequency region) for the flexibly coupled motor load system. Throughout the following investigation, a Runge-Kutta approximation was used to solve the descriptive differential equations of the system. This procedure is detailed in the following sections.

System Modeling

In the solution of the system differential equations, there are actually two subsystem equations to be solved. The mechanical system differential equations (see Appendices VI and VII), dealing with inertias, torques and viscous frictions must be solved simultaneously with the electrical system response equations describing voltage, currents, and torque output per phase (see Appendix IV). These equations form a coupled set of seven first order differential equations which must be solved in order to model the system (motor and load) response. The system of equations is somewhat complicated by the fact that the stator phases are assumed independent. This implies that only six of the differential equations actually affect the system response at a particular time. Two equations describe the motor, two describe the

load, while the remaining two describe the current (amperage) of the energizing and deenergizing stator phases. A subroutine (VOLTAG) was written to track the switching of the stator phases as a function of time. In the single step response modeling, this subroutine functions only once. In the multiple step model, it simulates the operation of the motor controller-driver. The six effective differential equations act as long as the current transients exist, after this point (transient quiescence) only five differential equations affect the system response. The general form for the main program for modeling of either single or multiple step response is constant. This is shown by the use of the program MODELP designed for the single step response as a subroutine MOTPSN for the multistep response (Appendices VIII and X). Consequently it is sufficient to examine the procedure for the construction of the single step modeling program (MODELP).

As is mentioned in the introduction to this chapter, a Runge-Kutta solution was written to model the step motor system. This is included in the main program MODELP. Following the suggestion of an excellent reference, (7), the actual system variables were displayed in state variable form in a function subroutine (FUNC). An explanation is necessary for interpretation of this procedure. X(1), X(2), and X(3) are the three stator phase currents, X(4) and X(5) are the motor position and velocity respectively, while X(6), and X(7) are the load position and velocity. Currents are described in amperes, position is in radians and velocity in radians per second. The step size for the R-K routine was determined by halving until three decimal accuracy was obtained. A step size of $.5 \times 10^{-4}$ was used in this program. Results of the Runge-Kutta

solution were displayed in two separate outputs. First pertinent variables were printed out by the computer for study. Later the state variables of the motor or load were displayed by means of a Calcomp plotter routine. This permitted visual comparison to the single step experimental results which were also processed by the program MODELP, (see Appendix IV). MODELP was a combinatorial program in that it operated on both the experimental points (by plotting) and on the theoretical data (calculation and display). In the case of the theoretical data, not every step of the Runge-Kutta routine was needed for plotting or print out. Consequently only pertinent (e.g. maxima) points were printed and plotted with a minimum of points between these critical points. Enough points were used to permit smooth plotting; however the goal was to minimize the expenditure of Input Output (I/O) time, and the storage space needed for plotting operations.

Although none of the programs of this investigation were initially designed as curve fitting programs, it was necessary to curve fit the theoretical single step response to the experimental results (Appendix IX). Consequently CFRICT and CFRIC2, the measured striction, and VFRICT, and VFRIC2 the calculated viscous friction (Appendix VII) were modified in the program MODELP. This modification was determined by arbitrary curve fitting procedures, including the reduction of the striction coefficient and the manipulation of the viscous friction coefficients. These modifications were made in successive program utilizing the system equations (Appendices VIII, IX, and X).

Separatrix Determination

The separatrix for a second order damped system precisely defines the regions of stability for that system. In the case of two coupled

second order systems, a true separatrix cannot be determined. However, if the rotor is viewed as an isolated second order system, it is possible to view the reaction of the load and the torque due to an active stator phase as a unusual forcing function for the second order rotor system. Under this viewpoint, it is possible to define a pseudo separatrix for the system as a whole which corresponds to the separatrix of the rotor. This pseudo separatrix is defined in terms of the rotor state variables, and defines regions of stability for the coupled system in terms of those variables.

When a single stator phase is active, an unstable system node exists 22.5 degrees of rotor rotation away from the aligned configuration for that phase. The program SEPTRX calculates the motor separatrix (system pseudo separatrix) by solving the system differential equations in reverse time, beginning at the unstable node (see Appendix I). Prior to the solution of the separatrix problem, the differential equations are manipulated utilizing a method suggested by Stoker (8). Although Stoker does not deal with this point, in actuality, the system can reach the unstable node point only in infinite time. Consequently a linearization about the unstable node point is necessary. This linearization provides the initial slope of the motor trajectory at the node point. Utilizing this slope, the first point is calculated back in time using the Runge-Kutta scheme. The program which executes these manipulations and displays the solution is presented in Appendix X. The method of solutions should be general, however, Stoker does not recommend use of the Runge-Kutta procedure, which may be restrictive. The results of SEPTRX were displayed as computer print out and as a computer plot (see Appendix IX).

The two identical traces of the separatrix for the motor state vector for a particular stable focus (spiral node) will bound a stable region for that focus. To obtain these stability bounds, the separatrix was solved (by SEPTRX) for a set of motor and load parameters and then shifted to the proper position for the stable focus under study.

Stability Investigation

The main impetus for the digital investigation is contained in the program SOLVE and its accoutrements, the subroutines FCN, FUNC, VOLTAG, READER, SEPTRX, MOTPSN, STABIL, and FREQCY (Appendices VIII, IX, and X). SOLVE, the main program functions as a calling program. It sequences and controls the operation of the various subroutines. SEPTRX, and MOTPSN are subroutines manufactured from previous main programs (MODELP and SEPTRX). FUNC and FCN are equivalent usages of the subroutines for state variable manipulation. VOLTAG is a modification of the single step version to permit multiple step operation as discussed above. READER is an input subroutine which concentrates all data manipulation in one subroutine. It is a dual entry point routine with a secondary entry at the point RESET. Entry into the subroutine at the point RESET causes the values of initialized variables to be reset. Such parameters as torque, time, phase current, etc. must be reset for each system run. STABIL is a processing program which compares the motor state variables at the time a successive step command is expected to the separatrix for a proper focus.

The proper stable focus is selected by the subroutines VOLTAG, and SEPTRX. VOLTAG controls the number of steps to be taken while SEPTRX adjusts the separatrix to the focus for the number of step commands input.

The comparison in STABIL which determines system stability is accomplished by comparing the velocity and position of the rotor to the previously selected separatrix at the time mentioned above. This determines stability of the system as a whole since the separatrix forms a bound for the stable region in the two dimensional state space of the rotor. This bounded area in two space is a projection of the four dimensional stable region of the coupled motor and load.

In this investigation five successive steps of rotor position were used, that is modeled in MOTPSN. Consequently the stable focus of interest is around the sixth step command position of 90 degrees. If the motor state vector is within the stable region around 90 degrees, subroutine STABIL outputs a positive one. The variable name for this output is STABLE. FREQCY, the next referenced subroutine is a frequency adjusting routine.

If STABLE (the variable) indicates a stable frequency, the pulse frequency is increased prior to recalculation of the motor state vector in MOTPSN. If an unstable frequency is indicated, (STABLE equal to minus one) the pulse frequency is decreased. As it is currently written, FREQ does not converge. A shift in the position of DELTA in the subroutine READER (to a point prior to the RESET entry point) would yield convergence. The nonconvergence caused an oscillation about the maximum predicted stable frequency for the lowest stable frequency region. The predictions of this program were tested for one set of experimental systems. This limited testing was necessary due to the excessive computer time requirements of the Runge-Kutta solution of a set of Differential Equations.

CHAPTER V

INVESTIGATION ANALYSIS

The following discussion follows the same format as the previous two chapters. The results for each segment of those chapters will be discussed sequentially and related to the overall aims of the investigation. However, it is important to note that a result not directly related to either experimentation or digital modeling was observed. As has been previously discussed, the digital programming and the experimental investigation proceeded concurrently. Thus early in the study, a commitment was made to the digital solution of multiple coupled differential equations as a system model. The pursuit of simultaneous inquiry into these cross related areas resulted in a somewhat inflexible research program. Since the experimental results were prerequisite to the final programming runs, this inflexibility was not apparent until the final stages of the investigation. At this point the excessive computer time demands of the Runge-Kutta integration approach were obvious. This time demand ranged upward from two minutes of U 1108 processing time for the solution of a single inertia load, spring rate system under the program SOLVE. While this in itself is not excessive, it is the minimum time for one of the 20 systems investigated experimentally. As the stable pulse frequency decreased, the computer time required expanded linearly at a high rate. Consequently only a minimum number of systems could be studied, due to computer time limitations, using this approach. The results for the limited number of systems which were analyzed under SOLVE are presented

below. The fact of interest is that Runge-Kutta solution of the numerous differential equations involved is too slow for wide application of this approach.

Discussion of Experimental Results

The preliminary investigation was primarily concerned with ascertaining the value of the inductance of the motor in the maximum and minimum L configurations. The results show that the voltage (and current) response times are at least an order of magnitude lower than the response of the mechanical system. As Robinson (9) points out, this implies that it should be possible to eliminate the current equations from the digital model. However, a review of the printed results of the modeling program resulted in the decision to retain the current variation in the system model. It was clear that the varying inductance in the motor made current perturbations more significant than in the case studied by Robinson, particularly in the first few steps of the Runge-Kutta integration (see Appendix IV).

The output of the photocell transducer is sketched in Figure 9, and the results of this transducer sensing are presented in Appendix V. There are several points to discuss pertaining to the output of this transducer under single step excitation. As was the case of the preliminary investigation, these results were primarily of interest in the determination of significant modeling parameters for the digital programming. The log decrement, the damped natural frequency, and the decay time following a single step command were determined from the photographs of system response. These parameters are displayed in Table 5. The single step experimentation also verified the two independent transducers sensing

Table 5. Single Step Response Results

Load in lbs 10^{2-5}	Spring Rate in lb/rad	W_d rad/sec	δ	Decay Time Experimental 10^{-3} secs	Theoretical 10^{-3} secs
0.0	00	448.799	.19641	139.3	160 >
3.1773	00	362.792	.17473	194.6	180
2.425	.533	150.571	.16502	209.8	215
"	1.066	173.78	.43371	236.6	250 >
"	2.133	208.299	.23411	258.9	280 >
"	4.267	251.267	.20103	287.5	270
5.5423	00	316.970	.20644	280.4	210
4.791	.533	125.947	.39051	225.0	230
"	1.066	144.960	.34660	241.1	240
"	2.133	160.223	.25358	275.0	280 >
"	4.267	208.190	.23518	275.0	280
25.472	00	171.64	.14544	571.4	520
24.720	.533	67.344	.31252	517.9	610
"	1.066	75.667	.233921	580.4	610 >
"	2.133	90.275	.15095	700.0	700 >
"	4.267	108.951	.15743	714.3	720 >
27.838					
27.838	00	162.147	.14684	666.1	510
27.091	.533	64.47	.34671	496.4	500
"	1.066	73.154	.2144	610.7	610 >
"	2.133	86.03	.17031	732.1	740 >
"	4.267	100.531	.16406	753.6	755

system vibration. The photocell and shutter provided a precise position sensing device. The magnetic vibration transducer provided a means of checking the time response of the phototransducer. Correlation of these two pickups was not possible since the magnetic device was velocity sensitive. However in evaluating the position sensing apparatus, the disagreement between the two devices regarding decay time was negligible.

The Multiple Step response results sought by the second segment of the investigation are presented in Table 6. The maximum stable frequencies for each region under study are actually the limiting frequencies as the command pulse frequency increases. Jump discontinuity in the frequency response was observed in determining these results, however only the increasing frequency stable limits were photographically recorded. The results confirm the existence of regions of stability bounded by unstable frequencies. It was found that a system could reach a stable excitation region bounded by unstable frequencies without unstable operation. When the input command frequency is constantly increased past the unstable frequencies, the motor remains in a stable mode of operation. The acceleration imposed by this procedure on the rotor and load drags the rotor through the unstable region. In this case the lag angle never becomes excessive and unstable operation is avoided. Included in Table 6 are the number of oscillations following a step command, prior to a succeeding command. This number is a qualitative measure of the nearness of the slew region of operation. In the slew region, no rotor oscillation will be observed. These results are also displayed in Figure 12, which demonstrates the interrelation of the spring rate, command frequency, and stable frequency limits for one load system.

Table 6. Multiple Step Response Results

Load in lbs^2 10^{-5}	Spring Rate	Maximum Stable Frequency p.p.s.		No. of Oscillations		Theoretical Stability Limit p.p.s.	
		Region 1	Region 2	Region 1	Region 2		
1.49524	00	31.75	45.26	3	2	27	32
0.74274	.533	25.2	43.87	2	1	25	30
"	1.066	19.7	27.55	3	2	19	24
"	2.133	22.3	30.6	3	2	22	27
"	4.267	25.4	36.2	3	2	25	30
3.8556	00	16.96	21.9	4	3	Not available	
3.1088	.533	9.4	13.6	3	2	"	"
"	1.066	10.5	14.99	3	2	"	"
"	2.133	12.1	12.5	3	2	"	"
"	4.267	14.3	20.66	3	2	"	"
23.7845	00	4.40	5.10	6	5	"	"
23.0377	.533	3.61	5.09	3	2	"	"
"	1.066	4.0	5.3	3	2	"	"
"	2.133	4.58	5.83	3	2	"	"
"	4.267	3.41	4.31	5	4	"	"
26.1505	00	4.4	5.1	6	5	"	"
25.4037	.533	3.42	5.05	3	2	"	"
"	1.066	4.36	5.74	3	2	"	"
"	2.133	3.36	4.17	3	2	"	"
"	4.267	3.42	5.05	5	4	"	"

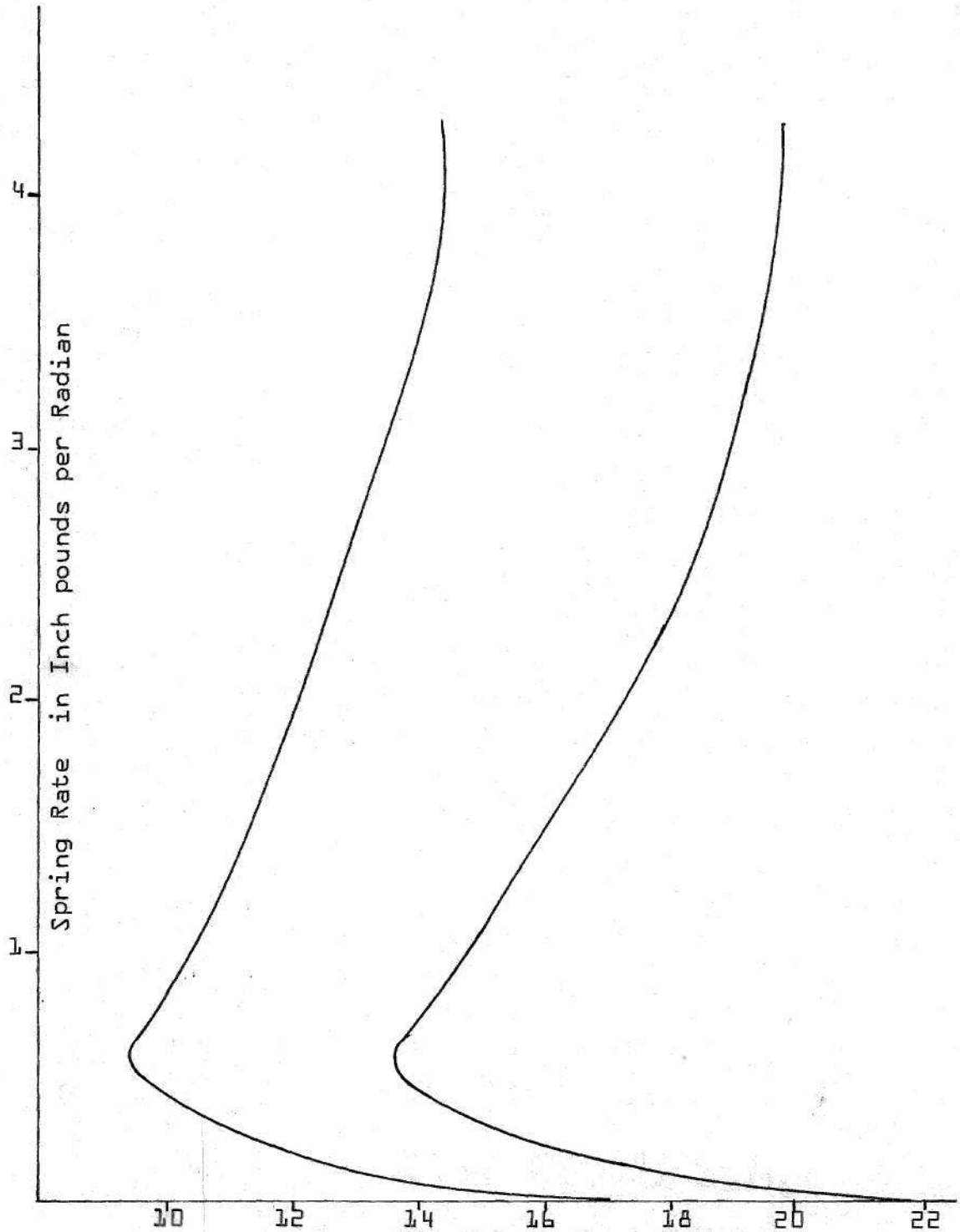

Figure 12. Maximum Stable Frequency Variation with Spring Rate

Figures 10 and 11 sketch the output display which was utilized in determining system stability. Figure 10 is a maximum stable frequency observed for the system indicated in stable region 1. Figure 11 is the same system, excited by a different frequency. The unusual response exhibited by Figure 11 should be compared to the response shown in Figure 28 of Appendix X. The same system is shown in each figure at slightly different frequencies. It was not possible to pursue the interesting similarity of these responses, however the resemblance lends credence to the capabilities of the digital model.

Discussion of Programming Results

The essential results of the digital programming effort are included in Appendices V, VIII, and X, and their accompanying figures. The modeling procedures surrounding the single step response have already been discussed and they are amplified in the pertinent Appendices (I, IV, VI, VII). The curve fitting results are displayed for two examples in Appendix VIII and finally in Appendix V. These plots are adequate to convey the success of the modeling adjustments made in the experimentally and theoretically determined parameters. The separatrix determination and its results are contained in Appendices IX and I. The results for these studies while significant will not be further discussed since for the purpose of this investigation, they were preliminary to the results obtained from the program SOLVE. The main program SOLVE brought the diverse elements mentioned above together in an attempt to digitally predict system instability.

The results of the SOLVE program are not conclusive, since they are incomplete. However, they are indicative of the success of the

procedure followed for the systems tested. These results are noted in Table 6, and indicate a high degree of correlation between the observed maximum stable frequencies for the first stable region and the frequencies predicted by the modeling comparison controlled by SOLVE. Under SOLVE, the digital model and the pseudo separatrix for the system are compared and a determination made on this basis of the system stability. It should be noted that the system of programs controlled under SOLVE selects the bounds for the stable frequency without manipulation by the programmer. As presented in Table 6 (under the heading "Theoretical Stability Limits), these results bracket the experimentally determined stability limits. However, in order to minimize the time required to converge to these bounds, a frequency near the experimentally determined maximum stable frequency was selected as a program starting point. It is still open to question how well this set of programs would predict stability for the system if the starting point was selected in a region bounded by unstable frequencies or at an extremely high value of step command frequency. Alternatively for the results which were obtained, the motor state vector lies close to the separatrix for the lower or upper limit determined by the program, depending on which limit is closer to the experimentally determined value. That is, the distance between the point in two dimensional state space which represents the motor state, at the time a succeeding step command is expected, and the nearest point of the system separatrix, is small. The system separatrix bounds the stable foci of the motor space, consequently a small difference implies that the values determined are near the limit possible for this program. Differences ranged from a minimum of 0.045

to a maximum of 1.4 radian per second. Intuitively the program should converge to these limits, however, as noted above this has not been demonstrated. In selecting the frequency bounds, the program was within five pulses per second of the experimental values. This result is the best possible with the convergence scheme used.

CHAPTER VI

CONCLUSIONS AND RECOMMENDATIONS

This chapter contains conclusions of a general nature which are supported by the results presented in Chapter V. The discussion will deal with the single step and the multiple step investigations in that order.

Conclusions From the Single Step Investigation

The conclusions which pertain to this area of investigation are preliminary to the discussion of multiple step comments. However the results of the single step response and model are interesting in their own right. The results demonstrate the direct dependence of system response decay time on system loading and flexibility. The decay time increased from a minimum of 139.3 milliseconds for the unloaded motor to a maximum of 753 milliseconds for the flexibly couped highest inertia system. Response decay time increases with decreasing flexibility; however the rigid coupling does not conform to this trend in all cases studied. The damped natural frequency observed increases with decreasing flexibility for all systems tested. The log decrement is dependent on both flexibility and the loading of the system. Higher loading decreased the log decrement as did increased rigidity in the coupling. The effective use of photocell transducer systems without the bias circuit is confirmed by the output of the magnetic transducer.

The modeling of the system single step response conforms to the observed response more precisely in the first few oscillations than in the final milliseconds of the decaying response. Modeling accurary in the first segment of the response is demonstrated by the computer plots. This matching appears to be a random function, i.e. it was not possible to correlate the matching precision and the systems under study. The feasibility of computer plotting of both experimental and theoretical results is demonstrated by the multiple plots of system response. Also demonstrated is the feasibility of utilizing the computer plotter for curve fitting, although this was not efficiently done in this investigation. The curve fitting procedures required to produce a good fit to the experimental results implies that the determination of modeling parameters for a coupled system requires further study. The match between the unloaded motor predicted response and the experimentally determined response indicates that in this case the procedures discussed were adequate. The mismatch displayed in other systems indicates that a better curve fitting approach is required.

Conclusions from the Multiple Step Investigation

The single step investigation formed the basis for the determination of the modeling parameters used in the multiple step model. Thus the quality of the matching in the first few oscillation of the single step response was of critical importance to the multiple step analysis. For the model used, the results indicate that the modeling was adequate. From the experimental results, it is clear that the maximum stable frequency for a system increases with increased rigidity and decreases with increased load for each stable region of excitation. It is important to

note that the nonlinear nature of the system caused jump discontinuities in the frequency response. The results presented are for an increasing command pulse rate. In all cases, the rigidly coupled system is unstable at a frequency farther from the slew frequency than any of the flexibly coupled systems, as is indicated by the number of oscillations between step commands. The modeling for all systems of the multiple step response are not correlated with the results of the experimentation. However, the computer plots shown for the single system examined indicate that the response predicted by the Multiple Step model will correlate well with the Multiple Step experimental results. This is due to the good agreement between the single step results and model. For the systems studied under the program SOLVE in an attempt to predict unstable regions, the region is bracketed to within five pulses per second by the program. In four cases, the bracket was upward, that is the observed maximum stable frequency formed the lower bound of the bracket interval. In one case, the program determined bracket was limited at the higher frequency by the experimental value. In each case, the distance between the rotor state vector and the separatrix was less than 1.4 radians per second at the frequency boundary nearest to the experimentally determined maximum stable frequency. The difference between the maximum stable frequencies bounding stable regions one and two decreased as the inertia load increased. This difference is a qualitative indication of the breadth of the stable region of operation. A final conclusion regarding the multiple step modeling and the stability determination is the inadequacy of the Runge-Kutta method for solution of the multiple differential equations involved

in this approach. The extravagant computer time demands of this approach (R-K integration) severely restricts its use for solution of a large number of systems.

Recommendations

The experimentation and modeling results open a wide range of possibilities for continued investigation. The general nature of this study leaves a large number of specific questions unanswered. On the theoretical level, several other approaches should be investigated. Particularly the use of Matrix state theory and the accompanying theorems on stability to define the stability limits for this system, and the use of a digital-analog model for the system should be investigated. Although the cost of such a model may be prohibitive, the results should be very indicative of the system response. The improvements on the method presented is relatively straightforward. A faster method of determining the system response either by a different solution scheme for the differential equations or by a different digital model is required prior to widespread use. One possibility for the improved model would be a direct curve fit to the single step response. A damped sinosoid should be definable for the response which would be adequate for the multiple step model. However a nonlinearity must be retained in the model for the definition of the separatrix which is influenced by the coupling of the load and the motor. Also an improved convergence technique for the alteration of command pulse frequency when the state vector is near the system pseudo separatrix is required. Finally the difficulty in defining experimentally the descriptive parameters of coupled differential equations suggests that further investigation into this area would be of interest.

APPENDIX I

The development of the equations describing the system is reserved for Appendices IV and VI; however it is appropriate to present at this point the mathematics supporting the FORTRAN programs SEPTRX and SOLVE which contain the theoretical predictions of this thesis. The determination of a two-dimensional separatrix for a four-dimensional system is a contradiction in terms. However since the system stability criterion is based on the values for the rotor state vector at a particular time, the following approach was deemed feasible.

The motor and the flexibly coupled load may be described by the following four state differential equations.

$$\frac{dx_1}{dt} = x_2 \tag{1}$$

$$\frac{dx_2}{dt} = \frac{\tau(x_1)}{J} - \frac{VF1\ x_2}{J} - \frac{CF1\ u_1}{J} - \frac{K\ (x_1 - x_3)}{J} \tag{2}$$

$$\frac{dx_3}{dt} = x_4 \tag{3}$$

$$\frac{dx_4}{dt} = \frac{-CF2\ u_2}{J_1} - \frac{VF2\ x_4}{J_1} - \frac{K\ (x_3 - x_1)}{J_1} \tag{4}$$

Where x_1 equals the motor position, x_2 equals the motor velocity, x_3 equals the load position, and x_4 equals the load velocity.

Dividing equations 2, 3, and 4 by equation 1 yields (as suggested

by Stoker (8)).

$$\frac{dx_2}{dx_1} = \frac{\tau\ (x_1)}{Jx_2} - \frac{VF1\ x_2}{Jx_2}\ \frac{-CF1\ u_1}{Jx_2} - \frac{K\ (x_1 - x_3)}{Jx_2} \tag{5}$$

$$\frac{dx_3}{dx_1} = \frac{x_4}{x_2} \tag{6}$$

$$\frac{dx_4}{dx_1} = \frac{-CF2\ u_2}{J_1 x_2} - \frac{VF2\ x_4}{J_1 x_2} - \frac{K\ (x_3 - x_1)}{J_1 x_2} \tag{7}$$

These equations (5, 6, 7) are amenable to solution by digital integration with the integration in terms of x_1, except for the lack of initial conditions. Only one set of initial conditions are available for the separatrix trajectory. The state vector values are known at any unstable equilibrium point, located 22.5 degrees from a stable aligned equilibrium configuration. In order to reach this point, the system velocity must decrease to zero over infinite time, while on the separatrix trajectory. By linearizing around the unstable point and stepping (integrating) in reverse time, a solution may be achieved. The linearization yields an initial value for the slope of the separatrix trajectory, which permits computation of the values of the state vector at a time short of infinity. The reverse time integration permits the value of the position of the rotor to be the integration variable under control of the Runge Kutta program.

Let $x_1 = .6544995$ $\quad x_2 = 0.0$

$x_3 = .6544995$ $\quad x_4 = 0.0$

Linearization of equation 5 implies

$$\frac{dx_2}{dx_1} = \frac{\overset{0.0}{\cancel{\tau(x_1)}}}{J\ \overset{0.0}{\cancel{x_2}}} - \frac{VF1}{J} - \frac{CF1}{J\ \overset{0.0}{\cancel{x_2}}} - \frac{\overset{0.0}{\cancel{K(x_1 - x_3)}}}{J\ \overset{0.0}{\cancel{x_2}}} \tag{8}$$

Due to the Coulomb Friction term, the trajectory approaches the x_1 axis along a perpendicular asymptote. Therefore this linearization will not yield the necessary starting points for the Runge-Kutta integration. Assume that the Coulomb friction is negligible at velocities close to zero on the perpendicular asymptote. Linearization about one of these points ($x_1 = x_3 = .6544995$; $x_2 = 0.0$) yields:

$$dx_2 = \frac{\overset{0.0}{\cancel{\tau(x_1)}}}{J\ x_2} - \frac{VF1}{J} - \frac{\overset{0.0}{\cancel{K(x_1 - x_3)}}}{J\ x_2}\ dx_1 \tag{9}$$

Therefore values for the result of the first step of the Runge-Kutta integration is given by:

$$x_{2,1} = \frac{-VF1\ H}{J}$$

where H is the step decrement on the rotor position variable. The Program SEPTRX which implements this scheme is presented in Appendix IX.

APPENDIX II

The usage of phototransducers is a complex and fascinating field of such scope that only a few remarks pertinent to their usage in this investigation are germane. The photocell used was rectangular, while the motion under study was rotational and therefore circular. Use of a circular shaped mask on the surface of the cell was considered in order to overcome this difficulty. However this implies that the cell is sensing positional variation in a range from full illumination of the sensitive area to complete masking of that area. At either extreme, the cell behaves nonlinearly. That is the voltage (or current output) is not proportional to the cell area remaining exposed. To overcome this problem common to photocell sensing devices two techniques were used.

The first technique, which is alluded to in the text, utilized a shunt resistor to ground in order to increase the cell current flow as the area illuminated varied. This technique merits further investigation, since a marked improvement in cell linearity was obtained by this approach. In conjunction with the shunt technique, the noise level normally associated with the use of photosensitive devices was reduced significantly by shielding all cable carrying sensing signals, and by working in D.C. source light only. This eliminated 60 cycle noise almost completely and reduced the effect of system noise to a negligible level.

The use of a rectangular cell without surface masking is justified

by examining the actual area variation as a function of the swept angle. As shown below, the area masked (covered by the shutter) varies as a combination of tangent functions. At fifteen degrees (.2618 radians) the tangent of fifteen degreen is .2679, a deviation of .0061 from a linear function of the angle. Examination of the cell and shutter used indicates that this is the theoretical deviation from linearity for the phototransducer.

Computation of the sensitive area was simplified by elimination of the upper and lower triangles of the cell which were either always masked or always exposed. Thus the area considered sensitive was a trapezoid swept by a shutter aligned with the centerline of this area.

Let j = Distance from the centerline of the shaft to the inside cell edge.

r = Distance from the centerline of the shaft to the outside cell edge.

θ = Angular variation of the shutter from the zero at at the upper triangle edge (if shutter is below cell centerline, θ = 45 degrees tan (θ) = 1).

$\emptyset$ = Angular variation of shutter below centerline ($\emptyset$ = 0.0 if the shutter is above centerline).

As the shutter is rotated from the $\theta = 0$ position past the cell centerline, the sensitive area swept out will be given by

$$\text{Area} = \tfrac{1}{2} (r^2 - j^2) \tan \theta + \tfrac{1}{2} (r^2 - j^2) \tan \emptyset \qquad (11)$$

Neither angle exceeds 14 degrees ($\tan \theta = .25$) of variation around the centerline of the cell since the cell dimensions dictate $\tan \theta_{max} =$

.75/r and for the system implemented r = 3.0, j = 1.875. This yields, for the area function describing the sensing area:

$$\text{Area} = 2.79\ (\tan \theta + \tan \phi) \qquad (12)$$

Therefore the cell area masked by the sweep of the shutter is a fairly linear function of the sweep angle (which equals $\theta + \phi$) of the shutter.

APPENDIX III

The calculation of the inertial loads and the spring rates for the system are straightforward. The presentation of the equations used for these parameters needs no amplification or discussion. However the calculations for the inertia of the shutter is a more interesting problem which merits complete development. The effect of the shutter inertia is marked in this system and points up the fact that in any experimentation, the interaction between the measuring apparatus and the parameter measured must be studied.

Shaft Inertia

$$I_a = \tfrac{1}{2} M_s R_s^2 \tag{13}$$

$$= \tfrac{1}{2} 1 \text{ Pi } R_s^2 \text{ p } R_s^2 \tag{14}$$

Load Inertia

Let M_t = Total mass; as if the slug were solid

M_i = Mass removed in drilling ¼" O.D. hole

M_s = Measured mass of the slug

$$p = M_x/(\text{Pi } 1 \ (R_o^2 - R_i^2)) \tag{15}$$

$$I_l = \tfrac{1}{2} M_t R_o^2 - \tfrac{1}{2} M_i R_i^2 \tag{16}$$

Let r = Radius of mounting shaft

R = Distance from the C.G., of the shutter to the outside of

the shaft.

q = Point of contact between the shaft and the dual knife edge support (instant center of rotation).

θ = Angular variation of shutter.

M_s = Mass of shaft.

Msh = Mass of shutter.

f = natural frequency = $w_n/2Pi$

The shutter inertia was calculated as if the shaft was eccentrically loaded by an inertia concentrated at the center of gravity for the shutter. The shaft was supported on parallel knife edges and the natural frequency of the shutter and shaft determined. These measurements and the calculations below yielded the shutter inertia. (see (10) and (11)).

$$M_q = I_q \frac{d^2\theta}{dt^2} = -M_{sh} g (R + r) \sin \theta \tag{17}$$

Approximating sin θ by θ yields

$$I_q + M_{sh} g (R + r) \theta = 0 \tag{18}$$

Solution of this differential equation implies

$$\theta = A \sin \left(M_{sh} \frac{g (R + r)}{I_q} t + \alpha\right) \tag{19}$$

Therefore

$$w_n^2 = M_{sh} g \frac{(R + r)}{I_q} \tag{20}$$

Applying the parallel axis theorem for inertias,

$$I_o = I_q - M_s r^2 - M_{sh} R^2 \tag{21}$$

$$I = \frac{M_{sh} g (R + r)}{w_n^2} - M_s r^2 - M_{sh} R^2 \tag{22}$$

For the shutters used

Unloaded motor:	$w_n = 13.69$ r/s	$M_{sh} = 2.11$ g.
	$r = .125$ in	$M_s = 4.99$ g.
	$R = .15$ in	
Loaded system:	$w_n = 13.404$ r/s	$M_{sh} = 2.6$ g.
	$r = .125$ in	$M_s = 30.3$ g.
	$R = 1.2$ in	

Spring Rates

The calculation of spring rates are based on standard formulas. These equations indicate that the flexure of the system was located entirely in the springs designed for the purpose of providing flexible coupling. All other shafts capable of flexible reaction acted rigidly under the small shear loads imposed by the system. For the springs used:

$$R_o = .0225 \text{ in}$$

$$G = \text{Shear modulus } 10.6 \cdot 10^6 \text{ psi}$$

$$K = \frac{G I_o}{\ell} = (10.6)\ (\text{Pi} R_o^4)\ (10^6)/2 \tag{23}$$

$$K = 4.267331440/1 \tag{24}$$

For the systems tested, ℓ equaled 1., 2., 3., and 4.

APPENDIX IV

In order to derive the descriptive differential equations for a step motor system, two simplifying assumptions were made. First, each phase or stator winding was analyzed as if it constituted a singly excited electrical system. Second, the inductance for each phase was assumed to be a function solely of the rotor position relative to the active phase. Clearly the second assumption is a consequence of the first, since for a singly excited coil, the only variation in inductance results from the movement of the rotor in the field of the coil. For a singly excited coil with a single low retentivity rotor pole in its magnetic field, the inductance will be given by

$$L_t = L + L_2 \cos \theta \tag{25}$$

where theta is the positional variation from the aligned position as shown in Figure 13. The two independent terms of the inductance may be associated with the constant air gap reactance and the varying reluctance caused by the rotor motion. For the multipolar stator and rotor configurations normally associated with step motors, this inductance equation must be modified. There are two methods of justifying this modification. Empirically, the multiple null points associated with several rotor and stator poles must be accounted for since there will exist several positions where reluctance is minimized and torque output is zero. Alternately, some means must be found to accomodate the disparity between mechanical and electrical degrees in the multi-

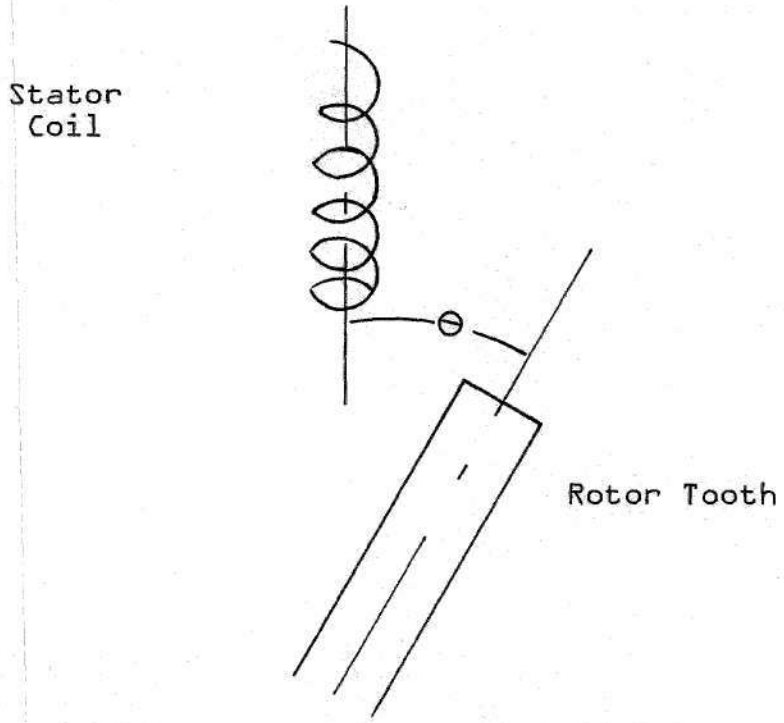

Figure 13. Schematic Singly Excited Coil

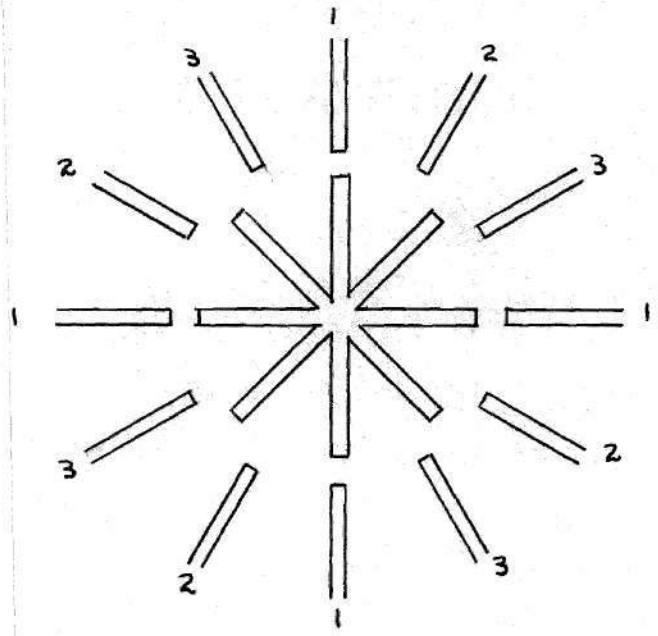

Figure 14. Schematic of Rotor and Stator Poles

polar system (12). For a motor with eight rotor poles and twelve stator poles, eight electrical radians equal one mechanical radian. Thus the inductance becomes:

$$L_t = L + L_2 \cos(n\theta) \qquad n = 8 \tag{26}$$

In general n will be given by:

$$n = 2\,Pi/(s\ a) \tag{27}$$

s = number of phases

a = size of step angle

As is shown in Figure 13, the rotor is displaced from phases 2 and 3 by plus or minus fifteen mechanical degrees when the rotor is aligned with phase 1. Theta, the angular displacement will be measured from this equilibrium position. Thus the inductance for phases two and three will be given by:

$$\text{For 2} \quad L + L_2 (\cos(n\theta - n\ 15)) \tag{28}$$

$$\text{For 3} \quad L + L_2 (\cos(n\theta - n\ 15)) \tag{29}$$

The constants L and L_2 must be determined experimentally for a specific motor. However they may be evaluated as:

$$L + L_2 = L_{max} \tag{30}$$

$$L - L_2 = L_{min} \tag{31}$$

From the experimentation surrounding the initial investigation, the values for L and L_2 may be calculated. These response time for the

voltage in the aligned and 22.5 degrees out of alignment configurations are T_1 = 160 μ sec, T_2 = 74 μ sec.

Thus

$$L = T \text{ Res.} \tag{32}$$

Implies

$$L_{max} = 3.2 \text{ mH}$$

$$L_{min} = .668 \text{ mH}$$

Therefore, L equals 1.934 mH and L_2 equals 1.266 mH.

As noted above, the current voltage relationship for each phase is assumed to be independent of the currents active in the remaining phases. Thus the application of Kirchoff's voltage law for the winding circuit implies:

$$V = R\, i + \frac{d(i\, L(\theta)}{d\, t} \tag{33}$$

$$= R\, i + \frac{di}{dt}\, L(\theta) + i\, \frac{dL(\theta)}{dt} \tag{34}$$

where $L(\theta)$ represents the complex inductance term. The second term on the right of equation 34 denotes the transformer or self induced electromotive force, while the final term represents the back EMF due to the changing rotor position. Inserting the previously derived equations for inductance, the equations describing the currents in each of the three phases are:

$$V_1 = R\, i_1 + \frac{di_1}{dt}\, (L + L_2 \cos\, (8\theta)) - i_1\, 8\, L_2 \sin 8\theta\, \frac{d\theta}{dt} \tag{35}$$

$$V_2 = R\, i_2 + \frac{di_2}{dt}\,(L + L_2 \cos(8\theta)) - i_2\, 8\, L_2 \sin 8\theta \frac{d\theta}{dt} \tag{36}$$

$$V_3 = R\, i_3 + \frac{di_3}{dt}\,(L + L_2 \cos(8\theta)) - i_3\, 8\, L_2 \sin(8\theta) \frac{d\theta}{dt} \tag{37}$$

These equations must be solved simultaneously for the transient currents in each of the stator phases as long as these transients are significant.

The torque output of a single phase of a variable reluctance step motor converts the electrical energy input to useful mechanical energy. The value of the torque output is determined by considering the energy stored in the magnetic field of the air gap and the conservation of energy. Clearly the input electrical energy will equal the increase in energy stored in the filled plus the mechanical work done. The electrical energy input is given by:

$$d(W_{elec}) = i \frac{d\lambda}{dt} dt \tag{38}$$

$$\lambda = L(\theta)\, i \tag{39}$$

$$d(W_{elec}) = id(L(\theta)i) \tag{40}$$

$$= i^2 d(L(\theta)) \tag{41}$$

When the phase current i is a constant value (implicitly assumed in equation 41), the energy stored in the field of the excited phase will be given by:

$$W_{fld} = \tfrac{1}{2}(i^2\, (L(\theta)) \tag{42}$$

Therefore

$$dW_{fld} = \tfrac{1}{2} i^2 \, d(L(\theta)) \tag{43}$$

The mechanical work done will be

$$dW_{mech} = \tau \, d\theta \tag{44}$$

The mechanical work must equal the difference of the input electrical energy and the energy stored in the field.

$$dW_{mech} = i^2 \, d\,(L(\theta)) - \tfrac{1}{2} \, i^2 \, d\,(L(\theta)) \tag{45}$$

$$\tau d\theta = \tfrac{1}{2} \, i^2 \, d\,(L(\theta)) \tag{46}$$

$$\tau = \tfrac{1}{2} \, i^2 \, \frac{d(L(\theta))}{d\theta} \tag{47}$$

The above equations coupled with the induction equation and the current voltage relationships provided a model of the torque output for each pole of the excited phase. When the phases are energized sequentially, the output torques will sum algebraically to yield:

$$\tau_1 = -4 \, i_1^2 \, L_2 \sin(8\theta) \tag{48}$$

$$\tau_2 = -4 \, i_2^2 \, L_2 \sin(8\theta - 120) \tag{49}$$

$$\tau_3 = -4 \, i_3^2 \, L_2 \sin(8\theta + 120) \tag{50}$$

$$\tau_{tot} = \tau_1 + \tau_2 + \tau_3 \tag{51}$$

Obviously the units of the torque must be adjusted to normally acceptable mechanical units thus,

$$\text{amp}^2 \, \frac{\text{Henry}}{\text{rad}} = \text{watt sec} \tag{52}$$

$$= 8.85072 \text{ in lb} \tag{53}$$

APPENDIX V

The figures included in this appendix need only minimal discussion. Plotted on the first two figures (15-16) are the theoretical state space response and the time response for the unloaded motor. As in the following figures, the time response included both the digitally predicted response and the experimentally determined response. The derivation of the modeling equations used which began in Appendix IV is further amplified in Appendices VI and VII. The program which executed the plotting routine and solved the digital model is presented in Appendix VIII.

These figures are the culmination of the curve fitting which was discussed in the text and is further discussed in Appendix VII. As such they represent the best approximation by the digital model to the actual system response to a single step command which was achieved by this study.

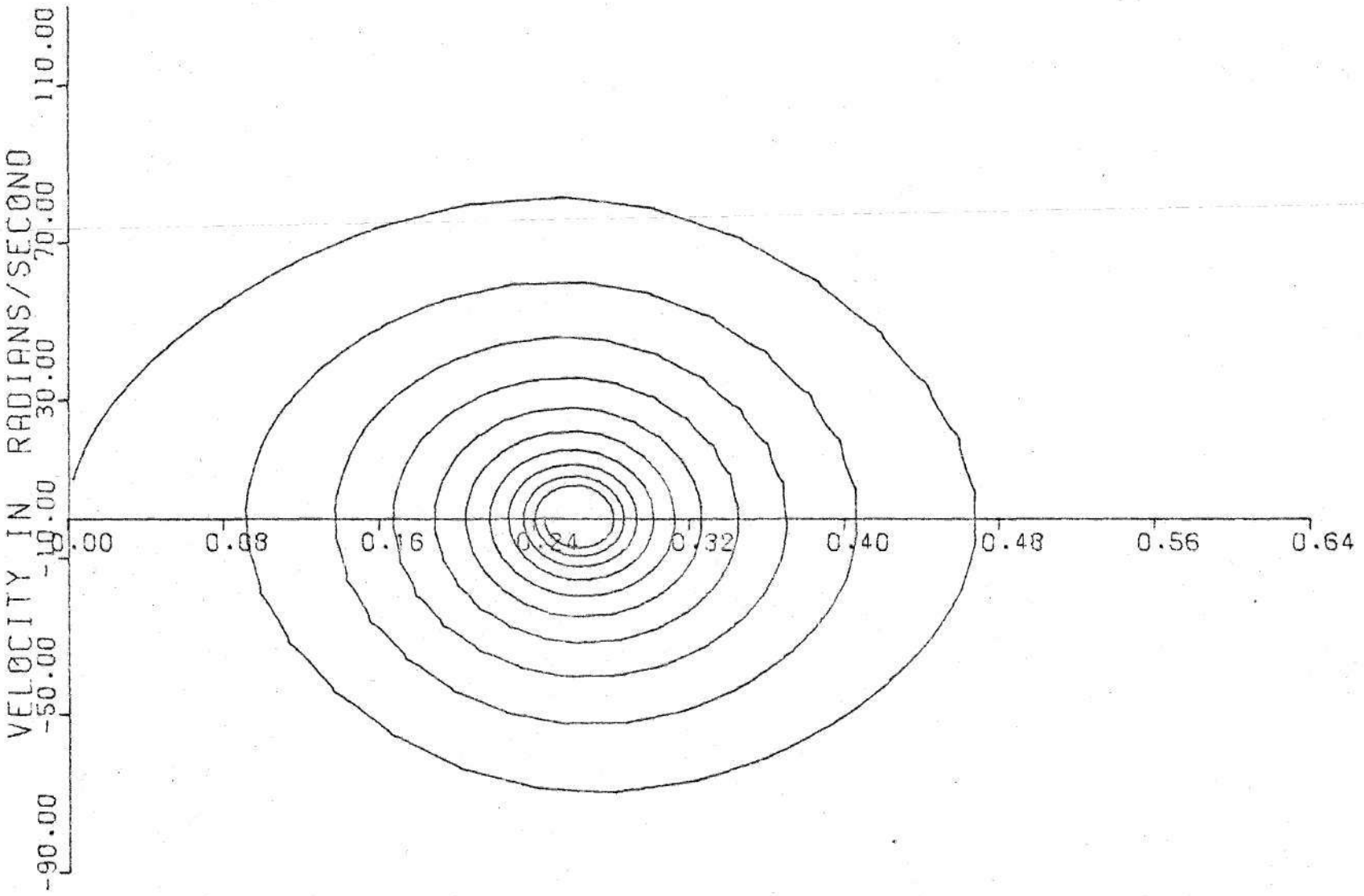

Figure 15. Unloaded Motor Single Step Response

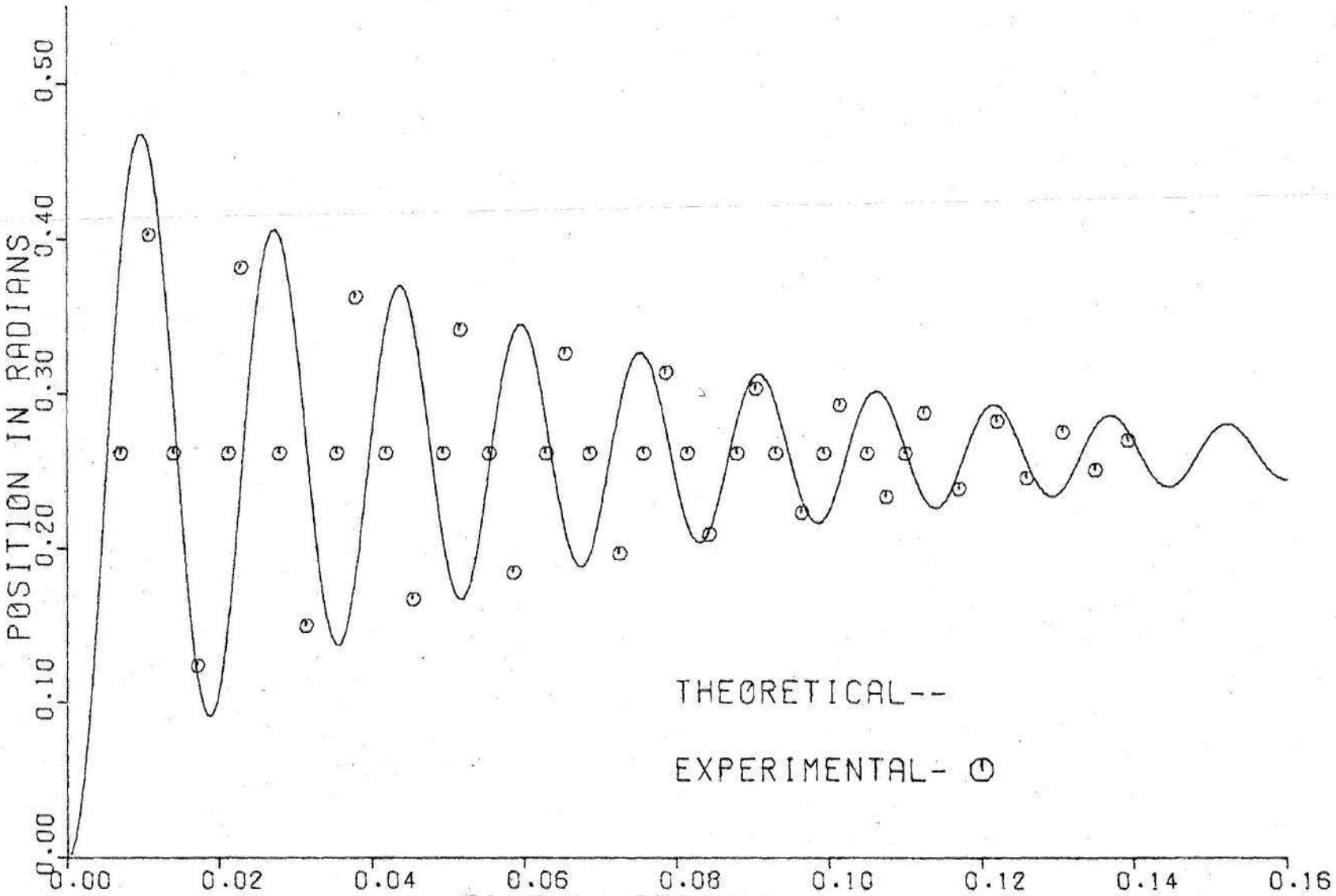

Figure 16. Unloaded Motor Single Step Response

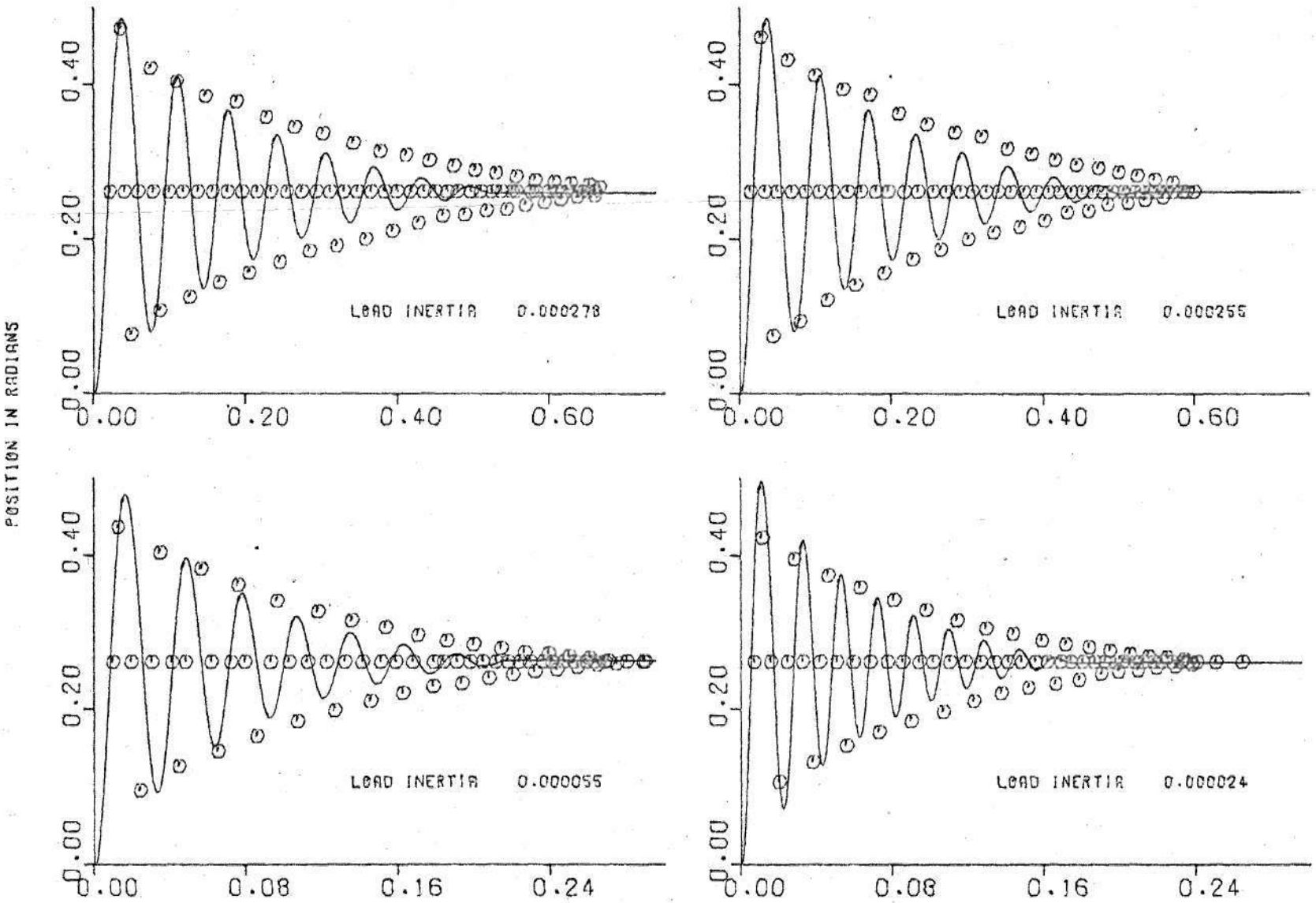

Figure 17. S. S. Response

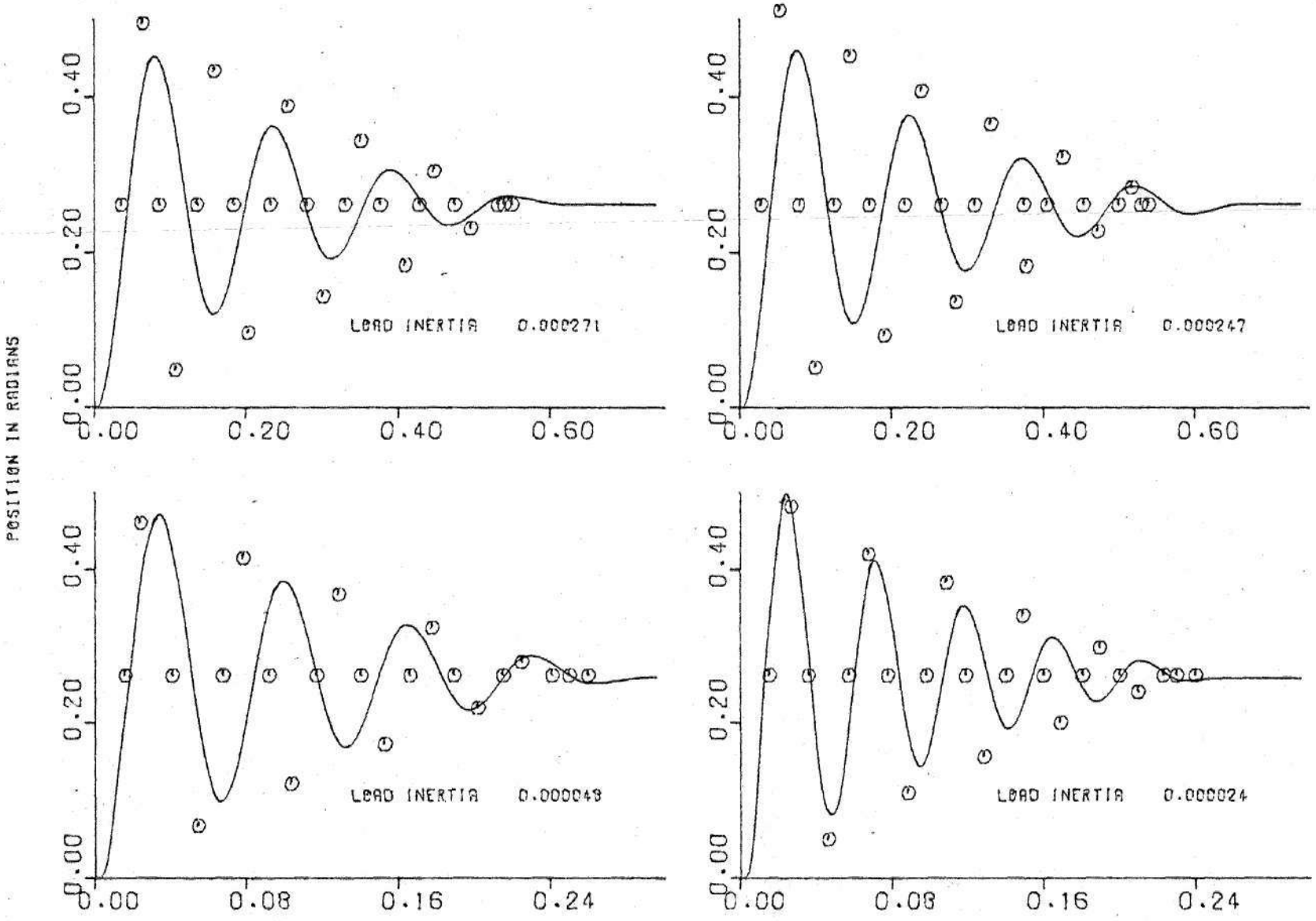

Figure 18. S. S. Response

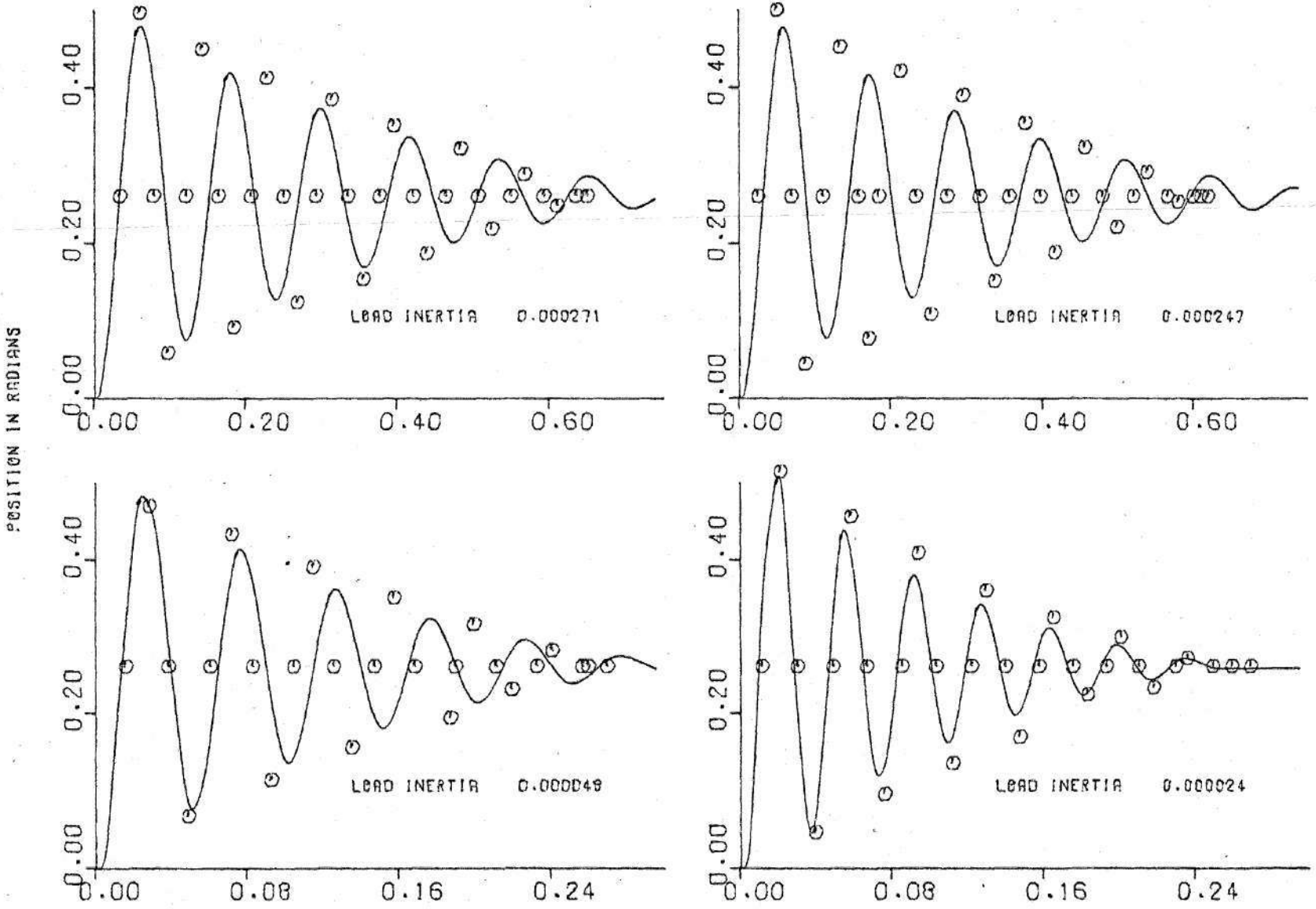

Figure 19. S. S. Response

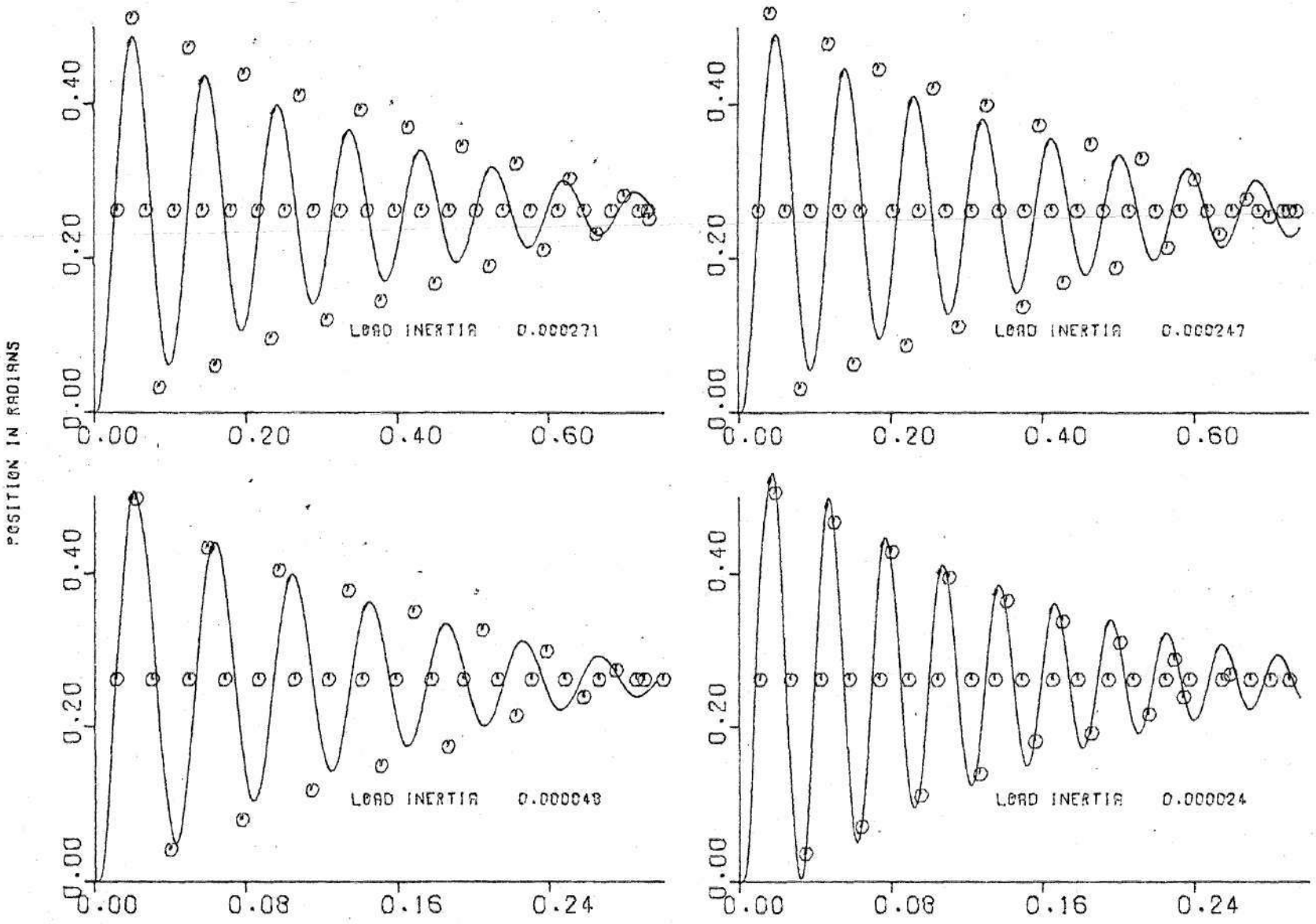

Figure 20. S. S. Response

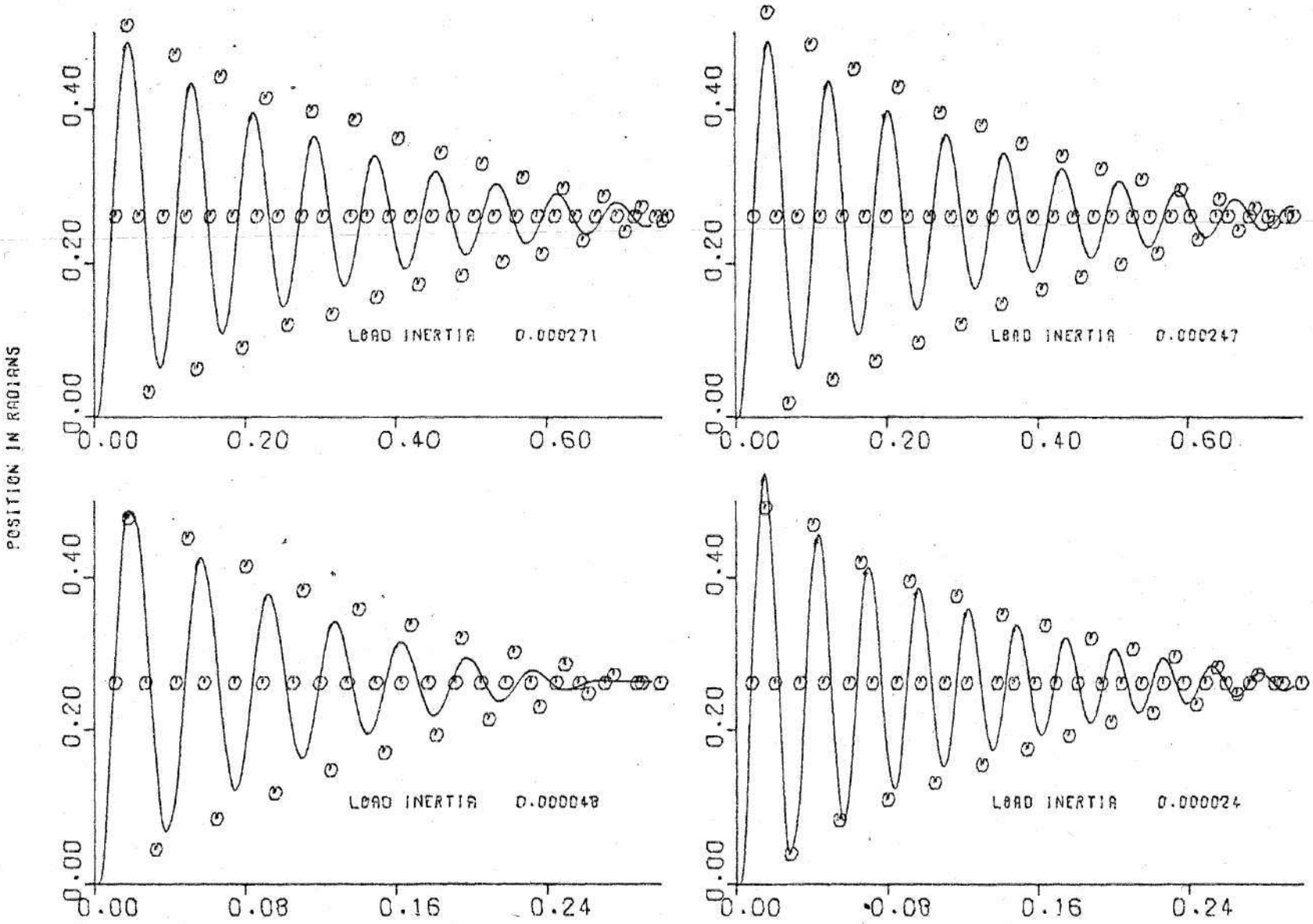

Figure 21. S. S. Response

APPENDIX VI

The unloaded motor, that is the system with no external load, may be described as a single rotational inertial acted upon by a complex torque, and opposing viscous and Coulomb friction. The equation describing this system may be determined by examination of Figure 22. That is,

$$\tau(\theta) = J\frac{d^2\theta}{dt^2} + CF1\left|\frac{d\theta}{dt}\right| / \frac{d\theta}{dt} + VF1\frac{d\theta}{dt} + K(\theta - \theta_2) \qquad (54)$$

Equation 54 will be applicable if the load and motor are rigidly connected. The values for CF1, VF1 and J will change when this type of loading is tested, but the format for the equation will remain unchanged. When the motor is flexibly coupled to the load the spring rate is non zero and a second descriptive differential equation is necessary in order to model the system.

$$0 = \frac{J_1 d^2\theta_2}{dt^2} + CF2\left|\frac{d\theta_2}{dt}\right| / \frac{d\theta_2}{dt} + VF2\frac{d\theta_2}{dt} + K(\theta_2 - \theta) \qquad (55)$$

It is obvious that equations 51 and 52 are the classical representation of the state differential equations presented in Appendix I. The resemblance between the system and a damped pendulum is more clearly shown in the classical format than in the state approach. The pendulum analogy for a step motor is quite good if the shift in stable point with command input is recognized. That is, a step motor in

the hold configuration resembles a pendulum possessing multiple stable foci. (The unloaded motor equation demonstrates this upon examination of the torque function.) When commanded to step, the stable point for the motor shifts by the displacement of successive stator phases. When the motor is flexibly coupled to the load, the analogy is less clear. The coupling of the motor inertia and the load inertia results in a fourth order system, which is difficult to model, particularly because of the digital nature of the torque function. For this reason, a digital computer was utilized to solve the system differential equations, and to track the requisite phase switching providing proper input torque.

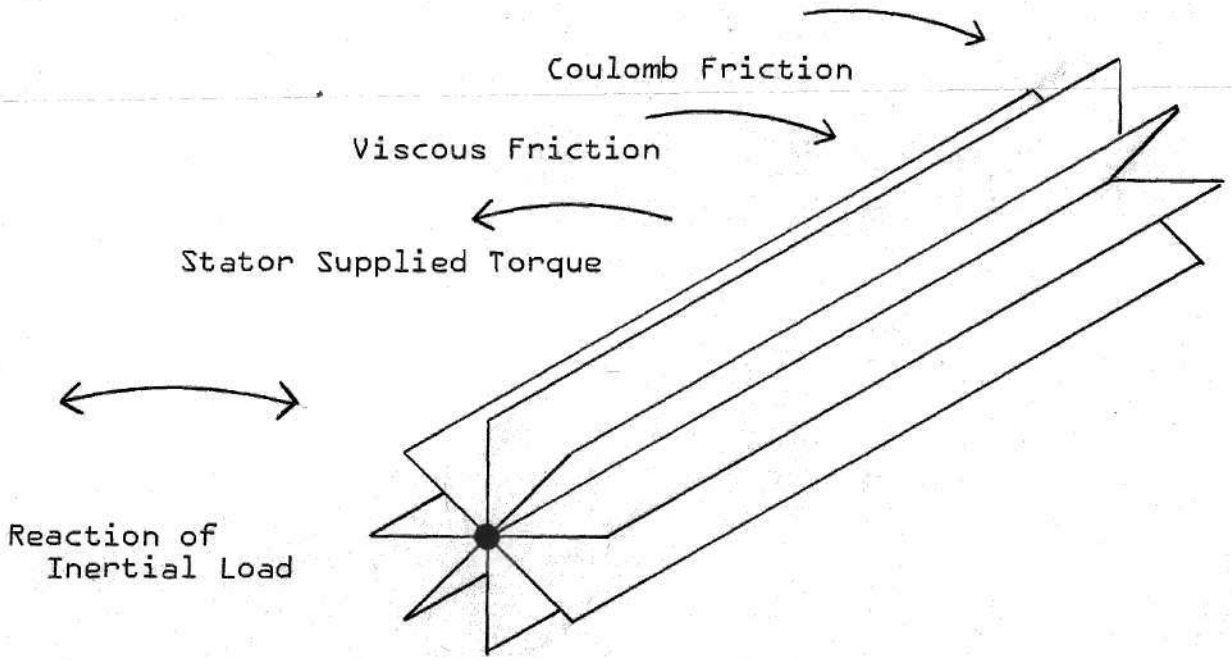

Figure 22. Free Body Diagram: Forces Acting on Rotor

APPENDIX VII

The equations presented in Appendices I and VI present some difficulties for the experimental definition of the model descriptive parameters. In the case of the unloaded motor, a relatively straightforward experimentation and data reduction scheme will yield the necessary parameters. In the case of the coupled system, a more complex approach is required. In either case, the experimental results referred to are the single step response photographs. By averaging successive overshoot and undershoot amplitudes, it was possible to determine the log decrement characteristic of the system tested (12). At the same time, an average damped natural frequency was determined for the system photographed. The ratio of the amplitudes yields:

$$\frac{z_i}{z_{i+1}} = \exp\left(\zeta w_n (t_2 - t_1)\right) \tag{56}$$

$$= \exp\left(\zeta w_n (2Pi/wd)\right) \tag{57}$$

The log decrement δ is given by

$$\delta = \ln\left(\exp\left(\zeta w_n (2Pi/wd)\right)\right) \tag{58}$$

From classical differential equation theory

$$w_n = w_d/\sqrt{1 - \zeta^2} \tag{59}$$

$$2 \zeta w_n = VF / J \tag{60}$$

Consequently solving equation (58) for δ yields

$$\delta = \frac{2Pi/W_n}{\sqrt{1 - \zeta^2}} \tag{61}$$

Solving equation (61) for implies

$$\zeta = \frac{\delta}{\sqrt{4\ Pi^2 + \delta^2}} \tag{62}$$

From equation (60)

$$VF = 2 \zeta w_n J \tag{63}$$

$$= \frac{2 \quad w_d J}{\sqrt{1 - \zeta^2}} \tag{64}$$

Therefore

$$VF = \frac{2\delta}{\sqrt{4\ Pi^2 + \delta^2}} \quad \frac{w_d \qquad J}{\sqrt{1 - \dfrac{\delta 2}{4\ Pi^2 + \delta^2}}} \tag{65}$$

Finally

$$VF = \frac{\delta\ w_d\ J}{Pi} \tag{66}$$

Equation (66) defines the viscous friction for the second order motor differential equation in terms of experimentally measurable parameters.

Identical measurements were made for the coupled system, the above computations yielded a value for the viscous friction of the coupled system. Use of this value which will be referred to as V3 for the system viscous friction would implicitly reduce the fourth order coupled system to a second order model. In order to derive parameter values for the fourth order digital model, it was assumed that V3 was a linear combination of VF1 and VF2, the motor viscous friction and the load viscous friction respectively. This assumption resulted in the curve fitting mentioned in the text. The value of the constant relating these three parameters was determined to be .75. Thus

$$VF2 = V3 - .75VF1 \tag{67}$$

Concurrently curve fitting for the values of the coulomb friction was pursued. The initial guess for the value of the Coulomb friction was the measured value of the stiction. This investigation resulted in a reduction of the stiction value by a factor of .125 as a model for the Coulomb friction in each part of the system. Thus the Coulomb friction was set at 12.5 per cent of the stiction measured experimentally.

APPENDIX VIII

This appendix contains the program MODELP which plotted the curves of Appendix IV and was utilized to plot the curve fitting results. Results of two sample curve fits are also included. The subroutines which accompany MODELP are presented as a necessary adjunct to the main program. The subroutine VOLTAG is presented in two formulations. The first for the single step test program, the second for the multiple step analysis. These subroutines and the program MODELP were elements of the main program SOLVE. MODELP was altered by changing the control cards from a main program to a subroutine for use by SOLVE. Thus it is presented in its entirety here and is not repeated in Appendix X. The subroutine name for MODELP for use by SOLVE is MOTPSN; the two names are interchangeable with regard to programming referenced by each name.

```
      Main Program MODELP
 1*   C  DATA FOR THIS PROGRAM MUST BE IN THE FOLLOWING ORDER1)RUNGE KUTTA
 2*   C  DATA INCLUDE H,B,T,FREQ,TORQUE,IPLOT$2) X(I) I=U,M$ 3) MOTOR INERTIA
 3*   C  INCLUDE RIGID COUPLING,COULOMB AND VISCOUS FRICTION,LOAD INERTIA S
 4*   C  RATE$ 4) EXPERIEMENTAL RESULTS TO BE PLOTTED
 5*        COMMON J,JLOAD,SPRGK,CFRIC2,VFRIC2,CFRICT,VFRICT
 6*        DIMENSION IBUF(6000),PSNPLT(1502),TIMPLT(1502),VELPLT(1502),TEXPLT
 7*       1(85),X1XPLT(85)
 8*        DIMENSION X(7),R(7,4),XB(7),XB1(7),XM1(7)
 9*        INTEGER ENDEX,M,COUNT
10*        REAL J,JLOAD
11*      1 READ 100,H,B,T,FREQ,TORQUE,IPLOT
12*        H=2.0*H
13*        IF(IPLOT.LE.0) GOTO 63
14*      100 FORMAT (2E10.5,3F10.5,I3)
15*        READ 101,(X(I),I=1,7)
16*      101 FORMAT (7F10.5)
17*        2 PRINT 201,FREQ
18*      201 FORMAT( 2X,18HPULSE FREQUENCY IS ,F10.5,6HP.P.S.  )
19*        PRINT 202
20*        PRINT 203,T,(X(I),I=1,5),TORQUE,(X(I),I=6,7)
21*      202 FORMAT (5X,4HTIME,4X,13HPHASE CURRENT ,30X,5HROTOR,9X,5HROTOR, 8X,
22*         16HTORQUE,8X,4HLOAD,10X,4HLOAD/18X,1H1,13X,1H2,11X,1H3,10X,8HPOSITI
23*         10N, 6X,8HVELOCITY,18X,8HPOSITION, 6X,8HVELOCITY)
24*      203 FORMAT (1X,E10.5,5E14.8,E10.5,2X,2E14.8,1X,I3)
25*        READ 103,J,CFRIC2,VFRIC2,JLOAD,SPRGK,CFRICT,VFRICT,DEL
26*   C  THE FOLLOWING STATEMENTS ADJUST PARAMETER VALUES TO CONFORM TO THE
27*   C  EXPERIMENTAL RESULTS.  SEE TEXT FOR DISCUSSION
28*        CFRICT=CFRICT*0.125
29*        CFRIC2=CFRIC2*0.125
30*        PRINT 205,J,CFRIC2,VFRIC2,JLOAD,SPRGK,CFRICT,VFRICT
31*        IF(IPLOT.GT.0) READ 103,IPTS,(TEXPLT(I),I=1,IPTS),(X1XPLT(I),I=1,I
32*       1PTS)
33*        PRINT 206,(TEXPLT(I),I=1,IPTS),(X1XPLT(I),I=1,IPTS)
34*      206 FORMAT (1X,11E11.5)
```

```
35*           COUNT=0
36*           INDEX=7
37*           IMDEX=1
38*           FACT=0.5
39*           XM1(4)=0.0
40*           M=0
41*           PI=3.14159265
42*           JPRINT=0
43*           JPLOT=0
44*           H2=H/2.
45*       205 FORMAT (7E14.8)
46*           IF(SPRGK.GT..1) GOTO 8
47*           LOAD1=4
48*           LOAD2=5
49*           GOTO 9
50*         8 LOAD1=6
51*           LOAD2=7
52*         9 VFRIC2=VFRIC2-FACT*VFRICT
53*           PRINT 205,J,CFRIC2,VFRIC2,JLOAD,SPRGK,CFRICT,VFRICT
54*        10 CONTINUE
55*     C  JPLOT CONTROLS INPUT POINTS FOR THE PLOTTING VECTORS, JPRINT CONTROLS
56*     C  THE PRINTER OUTPUT.
57*           IF(JPLOT.NE.3) GOTO 12
58*           JPLOT=0
59*           COUNT=COUNT+1
60*           TIMPLT(COUNT)=T
61*           PSNPLT(COUNT)=X(LOAD1)
62*           VELPLT(COUNT)=X(LOAD2)
63*           IF( COUNT.GE.1500) GOTO  50
64*           IF (JPRINT.LE.250) GOTO 12
65*           PRINT 203,T,(X(I),I=1,5),TORQUE,(X(I),I=6,7),COUNT
66*           JPRINT =0
67*        12 JPLOT=JPLOT+1
68*           JPRINT=JPRINT+1
69*           XM2=XM1(4)
70*           DO 13 I=1,7
```

```
71*          13 XM1(I)=X(I)
72*             TMAX=T
73*             TORKM=TORQUE
74*       C  BEGINNING OF THE RUNGE KUTTA ROUTINE
75*          21 DO 22 I=INDEX,ENDEX
76*             R(I,1)=FUNC(I,T,X,TORQUE,FREQ,M)
77*          22 XB(I)=X(I)+H2*R(I,1)
78*             TB=T+H2
79*             T=T+H
80*          27 DO 23 I=INDEX,ENDEX
81*             R(I,2)=FUNC(I,TB,XB,TORQUE,FREQ,M)
82*          23 XB1(I)=X(I)+H2*R(I,2)
83*             DO 24 I=INDEX,ENDEX
84*             R(I,3)=FUNC(I,TB,XB1,TORQUE,FREQ,M)
85*          24 XB(I)=X(I)+H*R(I,3)
86*             DO 25 I=INDEX,ENDEX
87*          25 R(I,4)=FUNC(I,T,XB,TORQUE,FREQ,M)
88*             DO 26 I=INDEX,ENDEX
89*          26 X(I)=X(I)+(H/6.)*(R(I,1)+2.*(R(I,2)+R(I,3))+R(I,4))
90*       C  END OF THE RUNGE KUTTA ROUTINE
91*       C  THIS SUBSECTION PROVIDES FOR MONITORING OF THE MAXIMUM AND MINIMUM
92*       C  VALUES OF THE POSITION VECTOR
93*             IF(ABS(XM1(4)-X(4)).LT.,150E-5) GOTO 29
94*             IF  ((XM1(4).GT.XM2.AND.XM1(4).GT.X(4)).OR.(XM1(4).LT.XM2.AND.XM1(
95*            14).LT.X(4)))  GOTO 28
96*             GOTO 29
97*          28 PRINT 204,TMAX,(XM1(I),I=1,5),TORQUE,(XM1(I),I=6,7),COUNT
98*         204 FORMAT(1X,E10.5,5E14.8,E10.5,1HM,1X,2E14.8,1X,I3)
99*             COUNT=COUNT+1
100*            TIMPLT(COUNT) =T
101*            PSNPLT(COUNT)=X(LOAD1)
102*            VELPLT(COUNT)=X(LOAD2)
103*         29 IF( COUNT.GE.1500) GOTO  50
104*            IF(T.GT.3.7*DEL) GOTO 50
105*            CMDPSN=M*PI/12.0
106*            GOTO 10
```

```
107*       50 CONTINUE
108*          PRINT 103,M,COUNT
109*          TIMPLT(COUNT+1)=0.0
110*          TIMPLT(COUNT+2)=DEL
111*          PSNPLT(COUNT+1)=0.0
112*          PSNPLT(COUNT+2)=0.20
113*          DO 30 K=1,IPTS
114*       30 X1XPLT(K)=X1XPLT(K)*PI/180.0
115*      103 FORMAT (      )
116*          GOTO (51,52,56,58,60),IPLOT
```

The FORTRAN statements following this segment pertain to functions proprietary to California Data Products Corporation, as such, they are not included in this presentation

```
1*          FUNCTION FUNC(I,T,,,TORQUE,FREQ,M)
2*          COMMON J,JLOAD,SPR,K,CFRIC2,VFRIC2,CFRICT,VFRICT
3*          DIMENSION X(7),V(3)
4*          REAL L,L2,K,J,JLOAD
5*    C  UNITS.      L,L2        HENRIES
6*    C              R           OHMS
7*    C              K           LB IN
8*    C              J           IN.LB.SEC.(2)
9*    C              VFRICT      IN.LB.SEC.
10*   C              CFRICT      IN.LB.
11*         L=.001934
12*         L2=.001266
13*         R=20.0
14*         EM=(FLOAT(M)-.00000001)/FREQ
15*         PI=3.14159265
16*         K=-8.85072*4.*L2*4.0
17*         EXP=2.0
18*   C  THE SUBROUTINE VOLTAG GENERATES THE STATOR COIL VOLTAGE.
19*         IF(M.EQ.0) ISTOP=0
20*      10 IF((T.GT.EM).AND.(ISTOP.NE.1)) CALL VOLTAG(V,M,ISTOP)
21*         DO 15 II=1,3
22*      15 IF (X(II).LT.1.0E-20)  X(II)=0.0
23*         GO TO (1,2,3,4,5,6,7 ) , I
24*       1 A=8.*X(4)
25*         FUNC=(V(1)-R*X(1)+X(1)*X(5)*8.*L2*SIN(A))/(L+L2*COS(A))
26*         RETURN
27*       2 B=A-2.0*PI/3.0
28*         FUNC=(V(2)-R*X(2)+X(2)*X(5)*8.*L2*SIN(B))/(L+L2*COS(B))
29*         RETURN
30*       3 C=A+2.0*PI/3.0
31*         FUNC=(V(3)-R*X(3)+X(3)*X(5)*8.*L2*SIN(C))/(L+L2*COS(C))
32*         RETURN
33*       4 FUNC=X(5)
34*         RETURN
35*       5 TORK1=K*SIN(8.*X(4))*X(1)**EXP
```

```
36*          TORK2=K*SIN(8.*X(4)-2.0*PI/3.0)*X(2)**EXP
37*          TORK3=K*SIN(8.*X(4)+2.0*PI/3.0)*X(3)**EXP
38*       31 TORQUE=TORK1+TORK2+TORK3
39*          IF(ABS(X(5)).GT..1E-25) GOTO 32
40*          UNIT= 0.0
41*          GOTO 33
42*       32 UNIT=ABS(X(5))/X(5)
43*       33 FUNC=TORQUE/J-(VFRICT/J)*X(5)-(CFRICT/J)*UNIT-(SPRGK/J)*(X(4)-X(6
44*         1) )
45*          RETURN
46*        6 FUNC=X(7)
47*          RETURN
48*        7 IF(ABS(X(7)).GT..1E-25) GO TO 34
49*          UNIT2=0.0
50*          GOTO 35
51*       34 UNIT2=ABS(X(7))/X(7)
52*       35 IF(ABS(JLOAD).GT..1E-25) GOTO 36
53*          FUNC=0.0
54*          RETURN
55*       36 FUNC=-(CFRIC2/JLOAD)*UNIT2-(SPRGK/JLOAD)*(X(6)-X(4))-VFRIC2*X(7)/J
56*         1LOAD
57*          RETURN
58*          END
```

```
      SUBROUTINE VOLTAG (V,M,ISTOP)
      DIMENSION V(3)
      INTEGER N
C  UNITS.     V(1),V(2),V(3),   VOLTS
      IF(M.EQ.0) ISTOP=1
      IF(M.EQ.0) N=1
      IF(N.NE.3) GOTO 11
      V(1)=28.
      V(3)=0.0
      GOTO 15
   11 IF (N.NE.2) GOTO 12
      V(2)=0.0
      V(3)=28.
      GOTO 15
   12 IF(N.GE.3) N=0
      V(1)=0.0
      V(2)=28.
      V(3)= 0.0
   15 CONTINUE
      M=M+1
      N=N+1
      PRINT 401,V(1),V(2),V(3),N,M
  401 FORMAT (2X,3F8.3,2I5)
      RETURN
      END
```

```
 1*          SUBROUTINE VOLTAG (V,M,ISTOP)
 2*          DIMENSION V(3)
 3*          INTEGER N
 4*    C  UNITS.     V(1),V(2),V(3),    VOLTS
 5*          IF(M.EQ.5) ISTOP=1
 6*          IF (ISTOP.EQ.1) RETURN
 7*          IF(M.EQ.0) N=1
 8*          IF(N.NE.3) GOTO 11
 9*          V(1)=28.
10*          V(3)=0.0
11*          GOTO 15
12*       11 IF (N.NE.2) GOTO 12
13*          V(2)=0.0
14*          V(3)=28.
15*          GOTO 15
16*       12 IF(N.GE.3) N=1
17*          V(1)=0.0
18*          V(2)=28.
19*          V(3)= 0.0
20*       15 CONTINUE
21*          M=M+1
22*          N=N+1
23*          PRINT 401,V(1),V(2),V(3),N,M
24*      401 FORMAT (2X,3F8.3,2I5)
25*          RETURN
26*          END
```

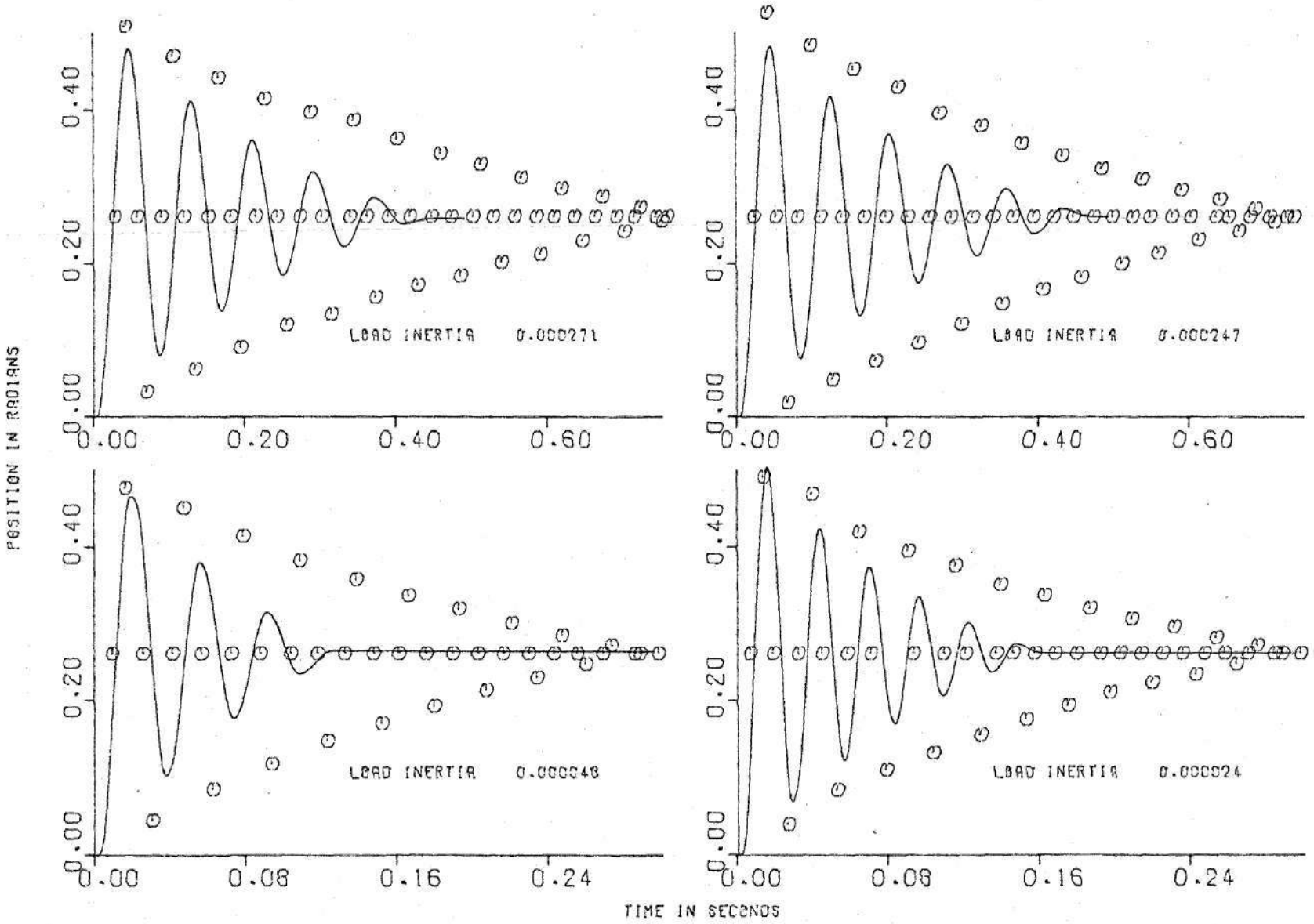

Figure 23. Curve Fitting Trial

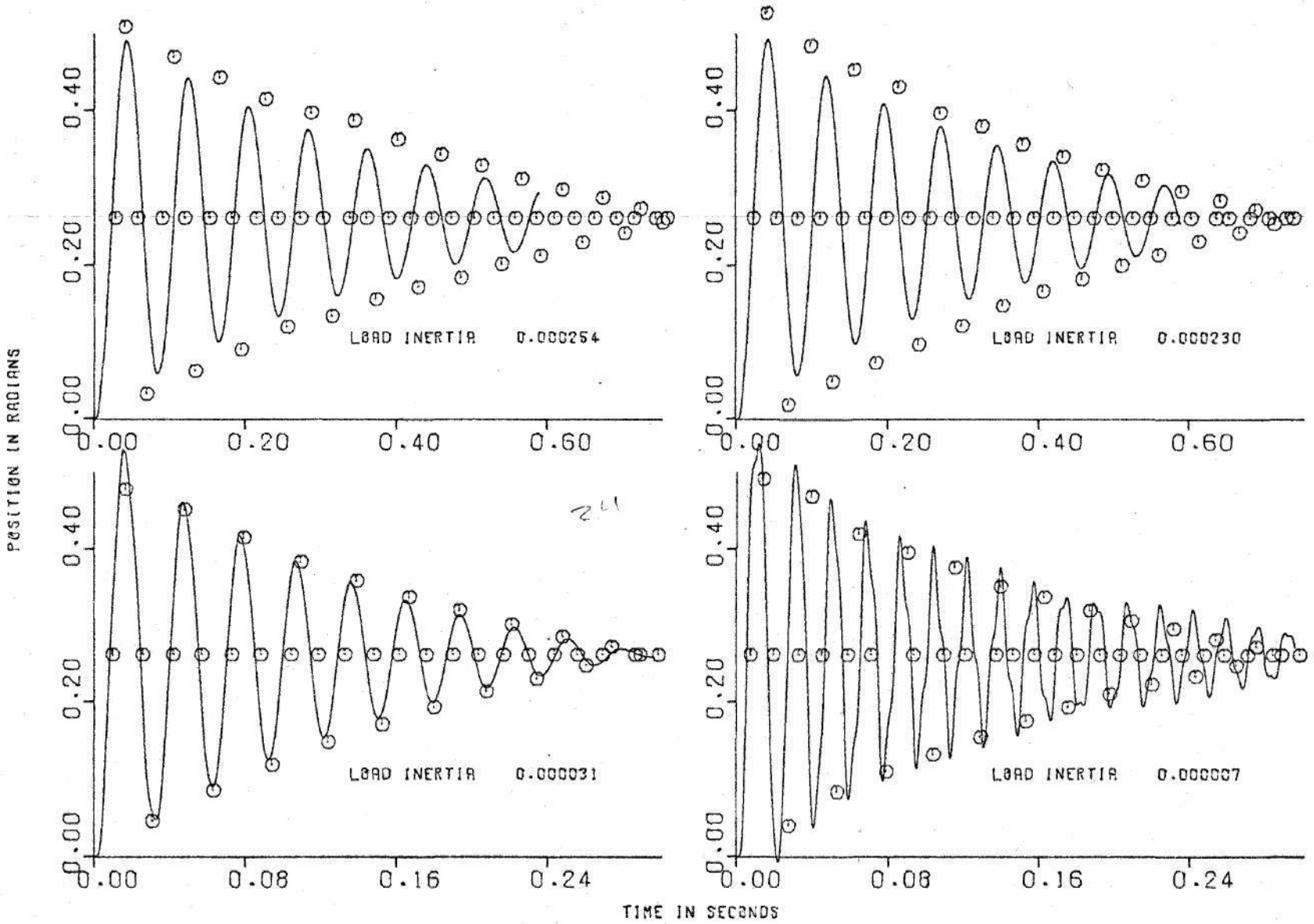

Figure 24. Curve Fitting Trial

APPENDIX IX

Presented below are the program SEPTRX and the trace of the system pseudo separatrix for one sample system which this program produced. The accompanying subroutine FCN is also presented. The main program SEPTRX was necessary for the program SOLVE as a subroutine (as was FCN). Since a minor change of control cards executes the alteration from main program to subroutine, the subroutine SEPTRX is not included in Appendix X.

```
                Main Program SEPTRX
   1*           COMMON TORQU, J,CFRICT,VFRICT,CFRIC2,VFRIC2,SPRGK,JLOAD
   2*           REAL J,JLOAD
   3*           DIMENSION X(3),R(3,4),XB(3),XB1(3),X1PLT(780),X2PLT(780)
   4*           DIMENSION IBUFF(5000)
   5*         1 READ 100,J,VFRICT,CFRICT,JLOAD,VFRIC2,CFRIC2,SPRGK
   6*           INTER=0
   7*         2 READ 101,H,B,X1,JPLOT
   8*       101 FORMAT (3F10.5,I3)
   9*           PRINT 100,H,B,X1,JPLOT
  10*           IF(JPLOT.LE.0) GOTO 500
  11*       100 FORMAT (     )
  12*           PRINT 200,J,VFRICT,CFRICT,JLOAD,VFRIC2,CFRIC2,SPRGK
  13*       200 FORMAT(9X,1HJ,10X,6HVFRICT,10X,6HCFRICT,10X,5HJLOAD,10X,6HVFRIC2,
  14*          110X,6HCFRIC2,10X,5HSPRGK//7(2X,F11.7,3X))
  15*       201 FORMAT (4X,9HMOTOR PSN,8X,9HMOTOR VEL,8X,8HLOAD PSN,8X,8HLOAD VEL,
  16*          18X,6HTORQUE,8X,5HCOUNT)
  17*       202 FORMAT (1X,4(E12.7,4X),E10.5,4X,I3,I7)
  18*           INTER = 0
  19*           IC=0
  20*           READ 100,(X(I),I=2,3)
  21*           FACT=0.50
  22*           VFRIC2=VFRIC2-FACT*VFRICT
  23*           CFRICT=CFRICT*0.125
  24*           CFRIC2=CFRIC2*0.125
  25*           X(1)=(VFRICT/J)*.01
  26*           PI=3.14159625
  27*           TORQU =-8.85072*4.0*.001266*4.0*1.4**2.0*(SIN(8.*.6444992-2.*PI/3.
  28*          1  ))
  29*           PRINT 201
  30*           X1PLT(1)=.65449922
  31*           X2PLT(1)=0.0
  32*           IPNTS=1
  33*           IPRINT=0
  34*           PRINT 202,X1,(X(I),I=1,3),TORQU ,IPNTS
```

```
35*           H2=H/2.0
36*           IF (IPNTS.EQ.1) GOTO 11
37*     C  BEGIN RUNGE KUTTA
38*         3 IF (X1.LT.-.2619) GOTO 10
39*           INTER=INTER+1
40*         4 DO 5 I=1,3
41*           R(I,1)=FCN(I,X1,X)
42*         5 XB(I)=X(I)+H2*R(I,1)
43*           X1B=X1+H2
44*           X1=X1+H
45*           DO 6 I=1,3
46*           R(I,2)=FCN(I,X1B,XB)
47*         6 XB1(I)=X(I)+H2*R(I,2)
48*           DO 7 I=1,3
49*           R(I,3)=FCN(I,X1B,XB1)
50*         7 XB(I)=X(I)+H*R(I,3)
51*           DO 8 I=1,3
52*         8 R(I,4)=FCN(I,X1,XB)
53*           DO 9 I=1,3
54*         9 X(I)=X(I)+(H/6.0)*(R(I,1)+2.0*(R(I,2)+R(I,3))+R(I,4))
55*     C  END OF RUNGE KUTTA
56*           IPRINT=IPRINT+1
57*           IF (IPNTS.LT.8) GOTO 11
58*           IF (IPRINT.NE.16) GOTO 3
59*        11 IPNTS=IPNTS+1
60*     C     X1PLT(IPNTS)=X1+(M-1)*.26179969
61*           X1PLT(IPNTS)=X1
62*     C     X2PLT(IPNTS)=X(1)+(M-1)*.26179969
63*           X2PLT(IPNTS)=X(1)
64*           IF(IPNTS.EQ.746) GOTO 10
65*           IPRINT=0
66*           PRINT 202,X1,(X(I),I=1,3),TORQU ,IPNTS,INTER
67*           GOTO 3
68*        10 CONTINUE
69*           PRINT 202,X1,(X(I),I=1,3),TORQU ,IPNTS
```

```
1*          FUNCTION FCN(I,X1,X)
2*          COMMON TORQU, J,CFRICT,VFRICT,CFRIC2,VFRIC2,SPRGK,JLOAD
3*          DIMENSION X(5)
4*          REAL J,JLOAD
5*          TORK=-8.85072*4.0*.001266*4.0*1.4**2.0
6*          PI=3.14159625
7*          ALPHA=(8.*X1 -2.*PI/3.)
8*          TORQU =TORK*SIN(ALPHA)
9*          GOTO (1,2,3),I
10*       1 IF(ABS(X(1)).GT.1E-25) GOTO 11
11*         UNIT=0.0
12*         GOTO 12
13*        11 UNIT=ABS(X(1))/X(1)
14*        12 FCN= TORQU/(J*(+X(1)))- VFRICT*X(1)/(J*(+X(1)))- CFRICT*UNIT/(J*(+
15*          1X(1)))-(SPRGK*(ABS(X1)-ABS(X(2))))/(J*(+X(1)))
16*         RETURN
17*       2 FCN=X(3)/(+X(1))
18*         RETURN
19*       3 IF(ABS(X(3)).GT.1E-25) GOTO 31
20*         UNIT2=0.0
21*         GOTO 32
22*        31 UNIT=ABS(X(3))/X(3)
23*        32 IF(ABS(JLOAD).GT.1E-25) GOTO 33
24*         FCN=0.0
25*         RETURN
26*        33 FCN=(-CFRIC2*UNIT2)/(JLOAD*(+X(1)))-SPRGK*(ABS(X(2))-ABS(X1)) /(JL
27*          1OAD*(+X(1)))-VFRIC2*X(3)/(JLOAD*(+X(1)))
28*         RETURN
29*         END
```

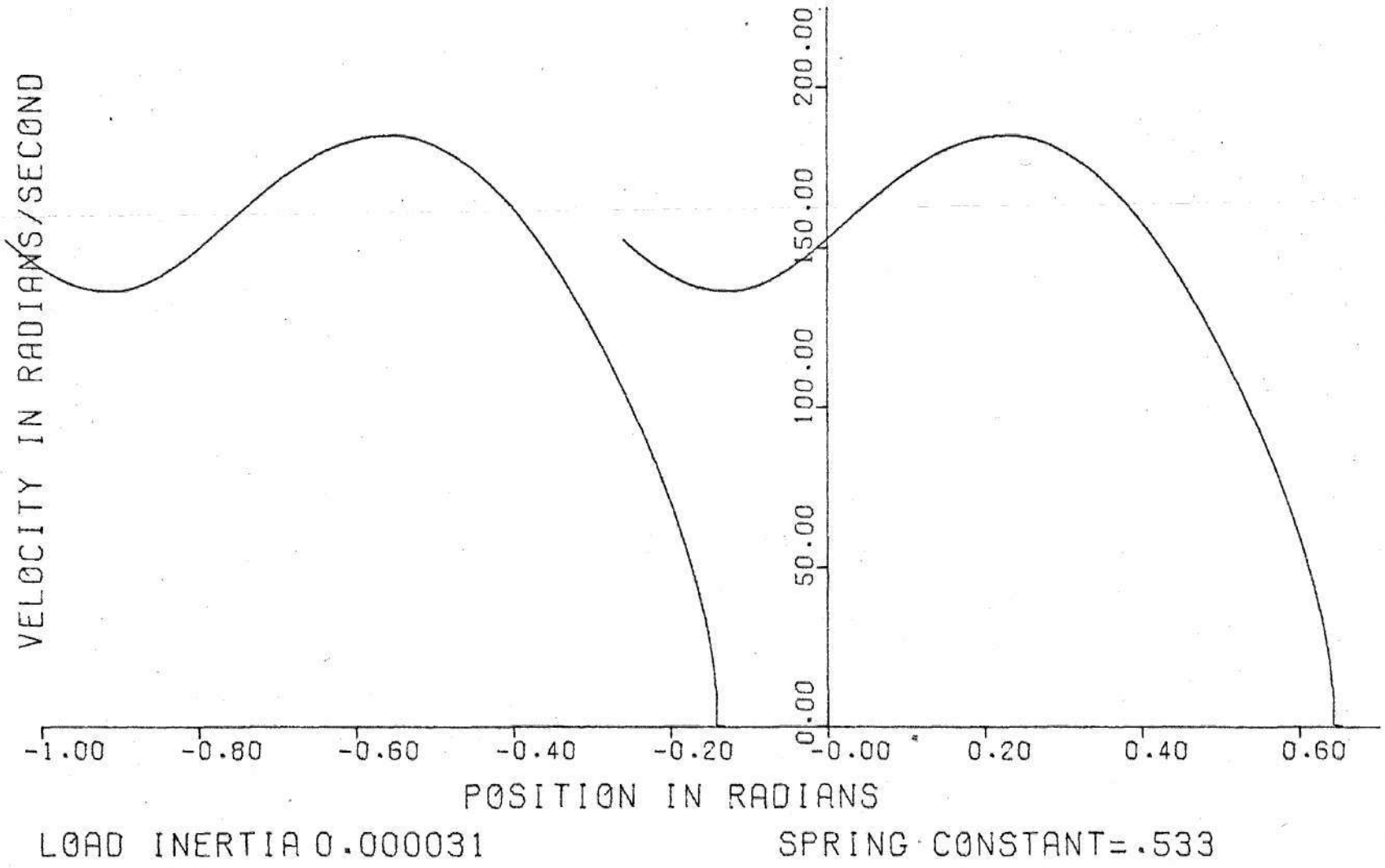

Figure 25. Trace of System Separatrix

APPENDIX X

The final program which draws together the results of the majority of the digital investigation is presented in this appendix. The program SOLVE combines elements of every aspect of the digital modeling and the experimental parameter determination. From this program, the digitally predicted limits for the stability regions were obtained. Also included are the multiple response predictions obtained by use of the multiple step version of VOLTAG. These plots are visual representation of the vector variation which SOLVE operated upon in determining the system stability.

```
      Main Program SOLVE
 1*   COMMON J,CFRICT,VFRICT,JLOAD,CFRIC2,VFRIC2,SPRGK
 2*   DIMENSION X(3),Y(7)
 3*   DIMENSION TIMPLT(780),VELPLT(780),PSNPLT(780)
 4*   DIMENSION X1PLT(780),X2PLT(780),XX1PLT(780),XX2PLT(780)
 5*   INTEGER COUNT
 6*   REAL J,JLOAD
 7*  200 FORMAT (19H STOPPED INTERNALLY  )
 8*    1 CALL READER(11,8,X1,HB,BB,T,TORQUE,FREQ,JSTOP,Y,X,DELTA)
 9*  C  JSTOP CONTROLS THE ENTIRE RUN
10*      INTER=.
11*      IF (JSTOP.LE.0) GOTO 500
12*    2 CALL SEPTRX(X1PLT,X2PLT,X1,H,B,JSTOP,M,XX1PLT,XX2PLT)
13*      IF(JSTOP.LE.0) GOTO 500
14*  C  ISTOP CONTROLS THE PULSE SOURCE
15*    3 CALL MOTPSN(PSNPLT,VELPLT,TIMPLT,Y,IPLOT,HB,BB,T,FREQ,M,COUNT)
16*    4 CALL STABIL(X1PLT,X2PLT,VELPLT,PSNPLT,COUNT,750,STABLE,FREQ,JSTOP,
17*     1M,DIST,XX1PLT,XX2PLT)
18*      IF(JSTOP.LE.0) GOTO 500
19*      INTER=INTER+1
20*  C  KSTOP CONTROLS THE FREQUENCY SEARCH
21*    5 CALL FREQCY(STABLE,FREQ,INTER,DELTA,KSTOP)
22*      IF (KSTOP.LE.0) GOTO 1
23*      CALL RESET(X1,T,TORQUE,Y,X)
24*      IF (INTER.GE.5) GOTO 600
25*      GOTO 3
26*  500 IF(JSTOP.EQ.0) STOP
27*      PRINT 200
28*      GOTO 700
29*  600 PRINT 201, INTER,FREQ,DIST
30*  201 FORMAT (1X,15HFREQUENCY AFTER ,I3,10HITERATIONS ,3X,E10.5,8H  P.P.
31*     1S.  ,5X,24HDISTANCE FROM SEPATRIX ,E12.8  )
32*      GOTO 1
33*  700 STOP
34*      END
```

```
      SUBROUTINE READER(H,B,X1,HB,BB,T,TORQUE,FREQ,JSTOP,Y,X,DELTA)
      COMMON J,CFRICT,VFRICT,JLOAD,CFRIC2,VFRIC2,SPRGK
      REAL J,JLOAD
  202 FORMAT(5X,1HJ,10X,6HCFRICT,7X,6HVFRICT,4X,5HJLOAD,6X,6HCFRIC2,8X,
     16HVFRIC2,6X,5HSPRGK)
      DIMENSION X(3),Y(7)
      PRINT 202
      READ 100,J,VFRICT,CFRICT,JLOAD,VFRIC2,CFRIC2,SPRGK
  100 FORMAT (    )
  201 FORMAT (1X,7E11.5)
      READ 101,FREQ
  101 FORMAT  (F10.5)
      PRINT 200, FREQ
  200 FORMAT (1X,12HFREQUENCY IS   ,F10.5,8H  P.P.S.  )
      READ 102, JSTOP
  102 FORMAT (I3)
      CFRICT=CFRICT*0.125
      CFRIC2=CFRIC2*0.125
      FACT=0.5
      VFRIC2=VFRIC2-FACT*VFRICT
      PRINT 201,J,CFRICT,VFRICT,JLOAD,CFRIC2,VFRIC2,SPRGK
      H=-0.1E-3
      B=.26179975
      HB=.1E-3
      BB=.4E0
      ENTRY RESET(X1,T,TORQUE,Y,X)
      DELTA=10.0
```

```
      X1=.65049922
      T=0.0
      TORQUE=0.0
      DO 1 I=2,7
    1 Y(I)=0.0
      Y(1)=1.40
      X(1)=.1E-10
      X(2)=0.0
      X(3)=0.0
      RETURN
      END
```

```
      SUBROUTINE STABIL(X1PLT,X2PLT,VELPLT,PSNPLT,COUNT,IPNTS,STABLE,
     1FREQ,JSTOP,M,DIST,XX1PLT,XX2PLT)
C  THIS SUBROUTINE DETERMINES STABILITY BY COMPARING THE MOTOR POSITION
C  TO THE PREVIOUSLY GENERATED SEPARATRIX
      COMMON J,CFRICT,VFRICT,JLOAD,CFRIC2,VFRIC2,SPRGK
      DIMENSION X1PLT(780),X2PLT(780),VELPLT(780),PSNPLT(780),XX1PLT(780
     1 ),XX2PLT(780)
      REAL J,JLOAD
      INTEGER COUNT,STABLE
      PI=3.14159625
      IPT=1
      IF (VELPLT(COUNT)) 10,4,1
    1 DIST=X1PLT(IPT)-VELPLT(COUNT)
      IF (DIST)2,3,3
    2 IPT=IPT+1
      IF(IPT.GE.IPNTS) GOTO 8
      GOTO 1
    3 IPT=IPT-1
      DELTA2=X2PLT(IPT+1)-X2PLT(IPT)
      PRINT 203, DIST,DELTA2
  203 FORMAT (1X,35HDISTANCE FROM SEPARATRIX VERTICALLY ,  E12.5,3X,6HDE
     1LTA2 ,E12.7  )
    4 IF (ABS(X1PLT(IPT)-PSNPLT(COUNT)).LT.PI/ 4.0)  GOTO 6
    5 STABLE=-1
      GOTO 7
    6 STABLE=+1
    7 PRINT 201,FREQ,STABLE
  201 FORMAT (1X,E12.5,2X,I3,16HSTABLE FREQUENCY  )
      RETURN
    8 PRINT 202
      JSTOP=-1
  202 FORMAT (1X,41HEXCEEDS LIMIT ON SEPARATRIX DETERMINATION  )
      RETURN
   10 DIST=XX2PLT(IPT)-VELPLT(COUNT)
      IF (DIST) 12,13,13
   12 IPT=IPT+1
```

```
*          IF (IPT.GE.IPNTS) GOTO 8
*          GOTO 10
*       13 IPT=IPT-1
*          DELTA2=X2PLT(IPT+1)-X2PLT(IPT)
*          PRINT 203, DIST,DELTA2
*       14 IF (XX1PLT(IPT)-PSNPLT(COUNT)-PI/12.0) 15,16,16
*       15 STABLE=-1
*          GOTO 7
*       16 STABLE=+1
*          GOTO 7
*          END
```

```
    1*          SUBROUTINE FREQCY(STABLE,FREQ,INTER,DELTA,KSTOP)
    2*    C  THIS SUBROUTINE CAUSES AN INCREASE OR DECREASE IN THE FREQUENCY
    3*    C  DEPENDANT ON THE DETERMINATION OF THE ROUTINE STABIL
    4*          COMMON J,CFRICT,VFRICT,JLOAD,CFRIC2,VFRIC2,SPRGK
    5*          INTEGER STABLE,STABL1,STABL2
    6*          REAL J,JLOAD
    7*          KSTOP=+1
    8*          IF(INTER.NE.1) GOTO 2
    9*        1 FREQ1=0.0
   10*          STABL1=0
   11*        2 FREQ2=FREQ1
   12*          STABL2=STABL1
   13*          FREQ1=FREQ
   14*          STABL1=STABLE
   15*          IF(STABL1.NE.STABL2) GOTO3
   16*          IF(ABS(FREQ2-FREQ1).GT.1.0) GOTO 3
   17*          PRINT 201,FREQ,INTER
   18*          KSTOP=-1
   19*          RETURN
   20*        3 DELTA=DELTA/2.0
   21*          IF (DELTA.LT..5) DELTA=0.5
   22*          FREQ=FREQ+STABLE*DELTA
   23*          PRINT 202,FREQ,INTER
   24*          IF (FREQ.LT.0.0) GOTO 4
   25*          RETURN
   26*        4 PRINT 203
   27*          KSTOP=-1
   28*          RETURN
   29*      201 FORMAT(1X,15HMAX STABLE FREQ,F10.5,17HSTEPS TO CONVERGE ,I3)
   30*      202 FORMAT(1X,12HCURRENT FREQ  ,E12.5,13HSTEPS CURRENT  ,I3)
   31*      203 FORMAT (1X,22HFREQUENCY OUT OF RANGE  )
   32*          END
```

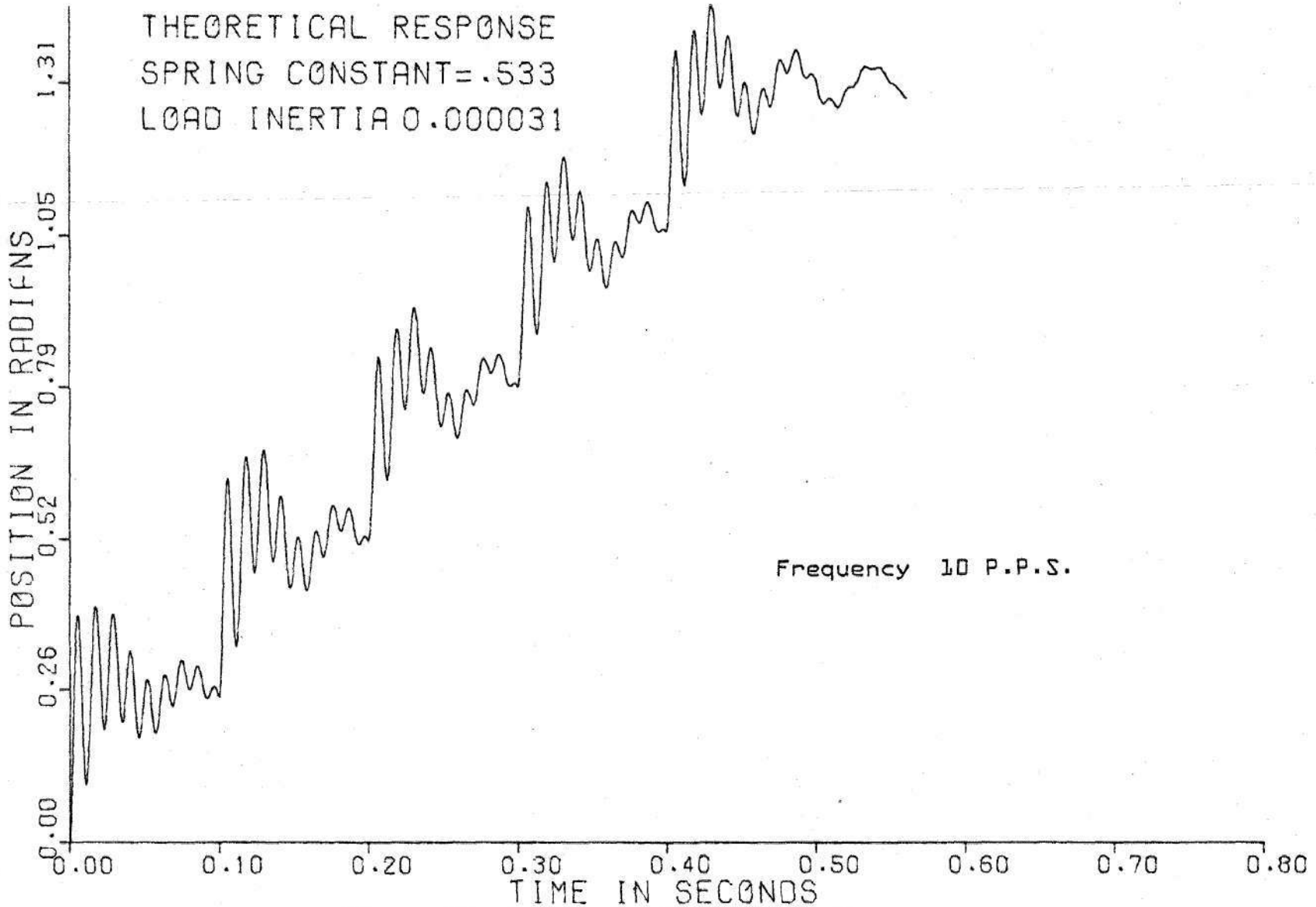

Figure 26. System M. S. Time Response

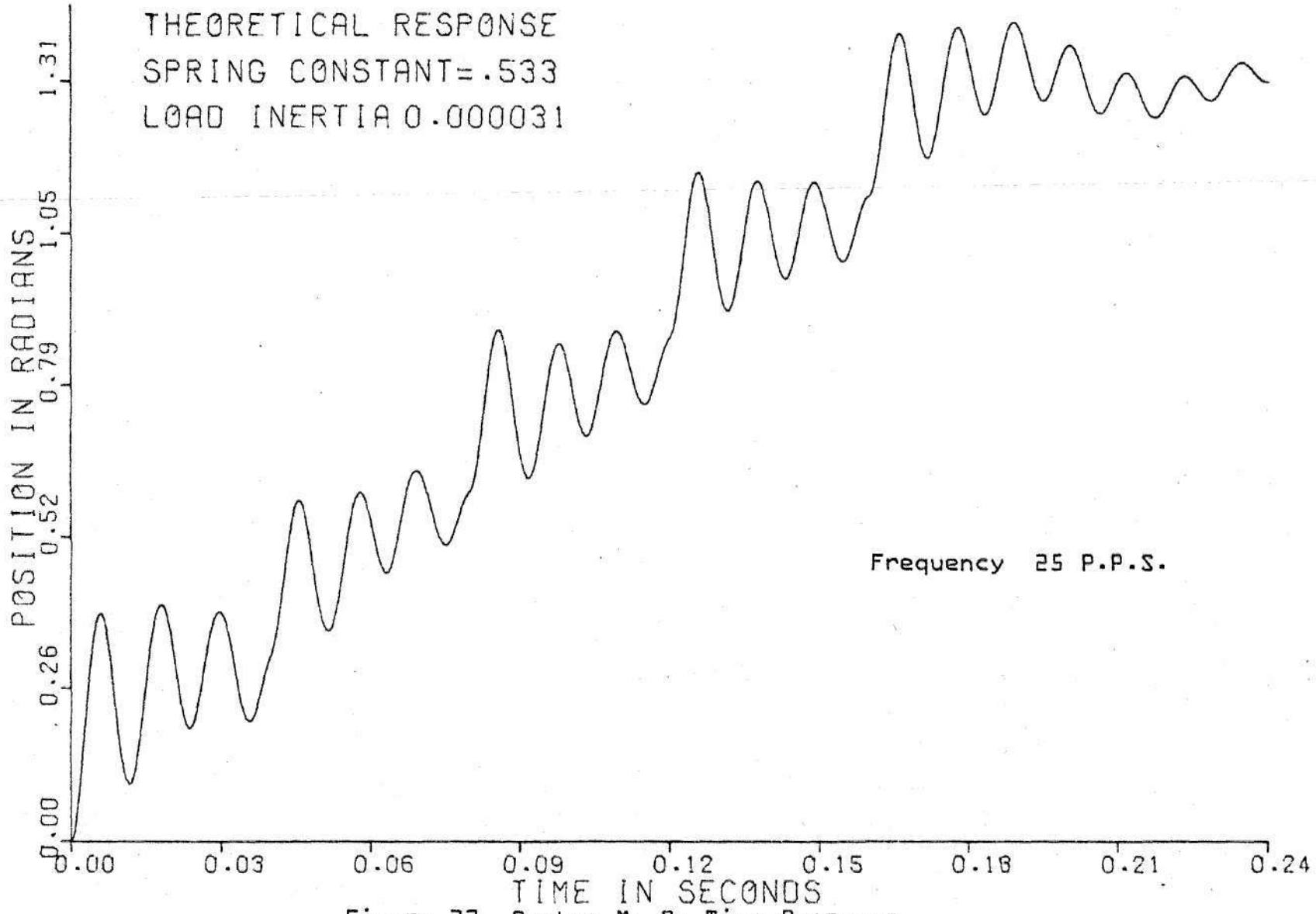

Figure 27. System M. S. Time Response

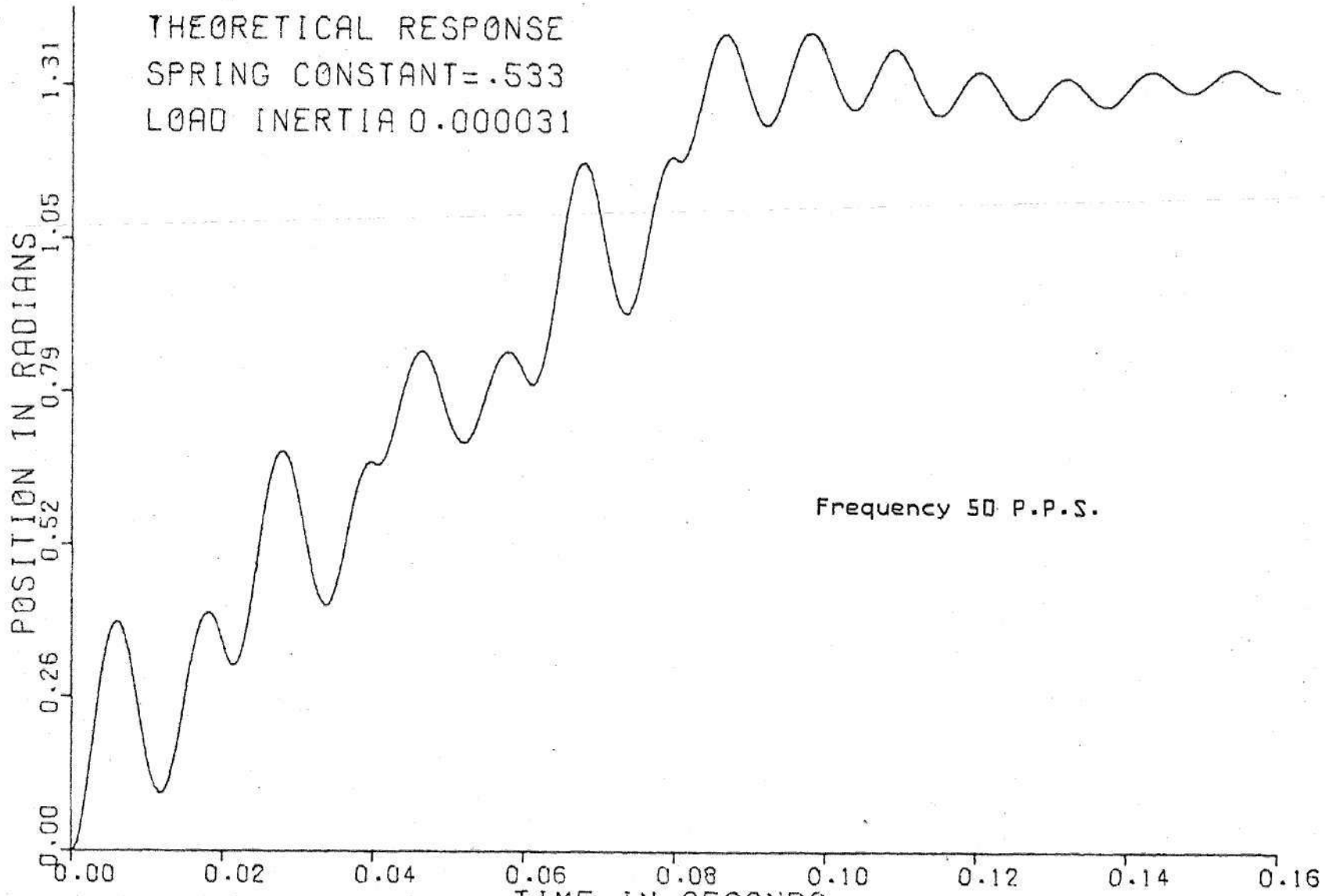

Figure 28. System M. S. Time Response

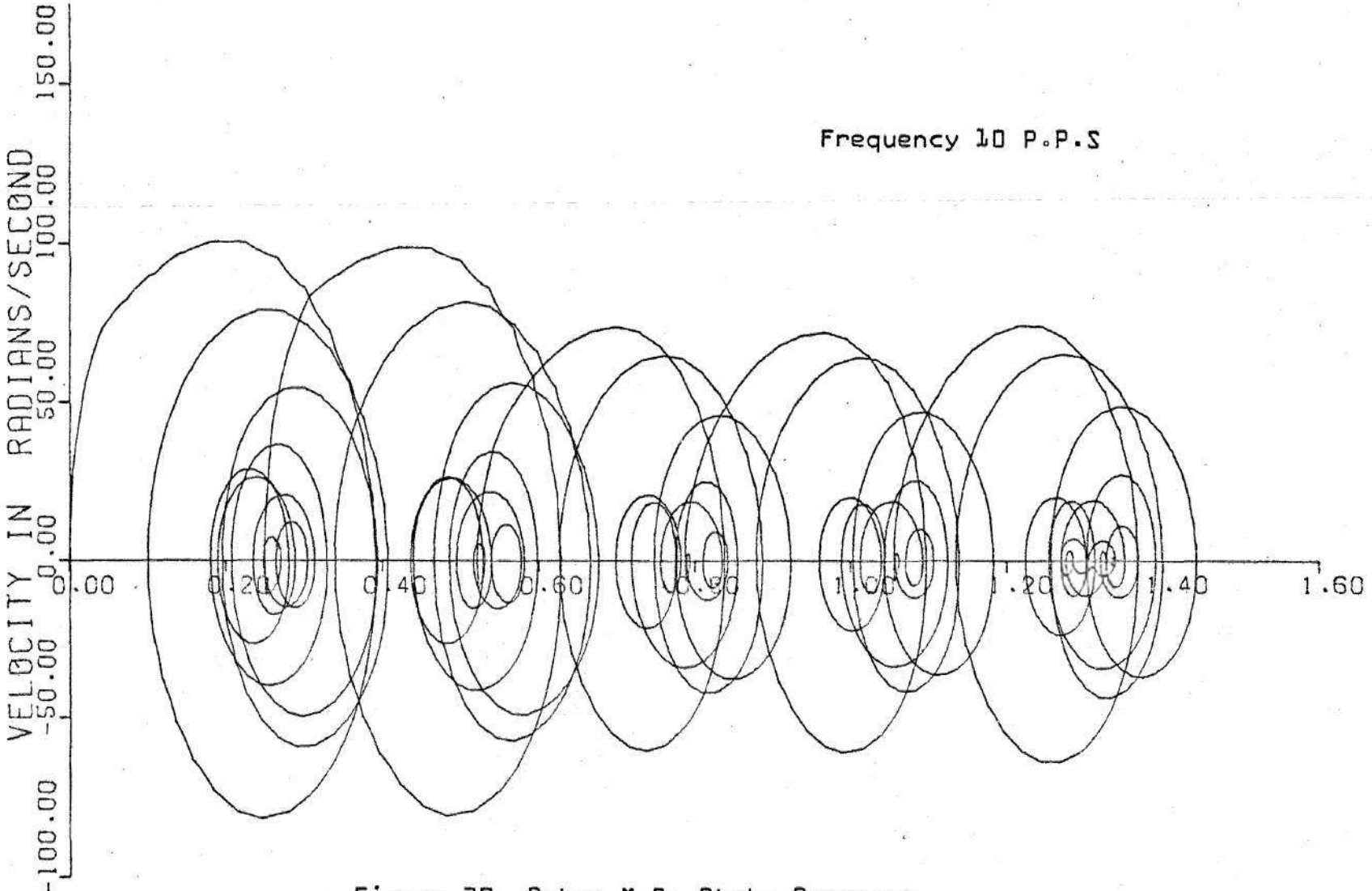

Figure 29. Rotor M.S. State Response

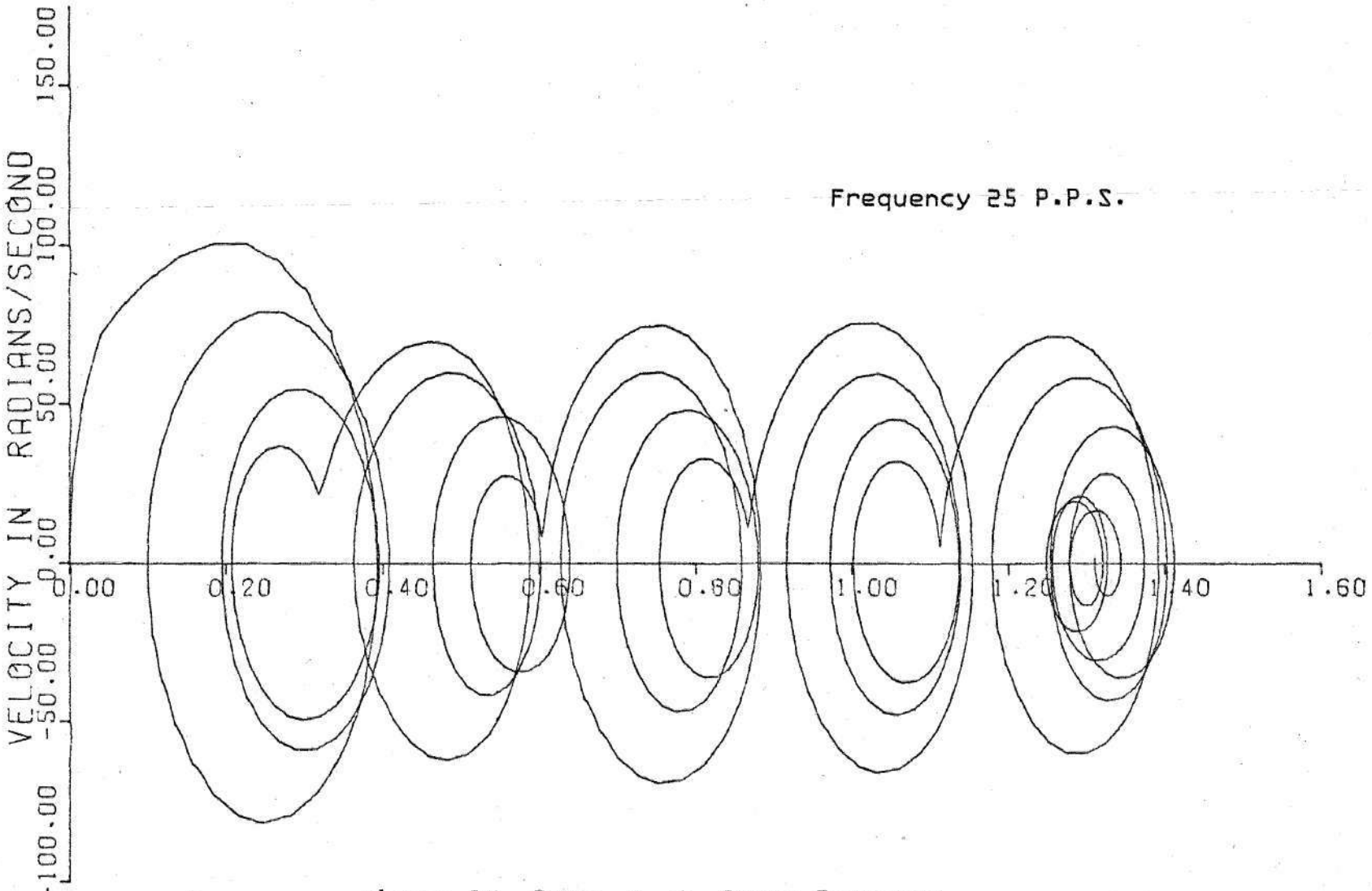

Figure 30. Rotor M. S. State Response

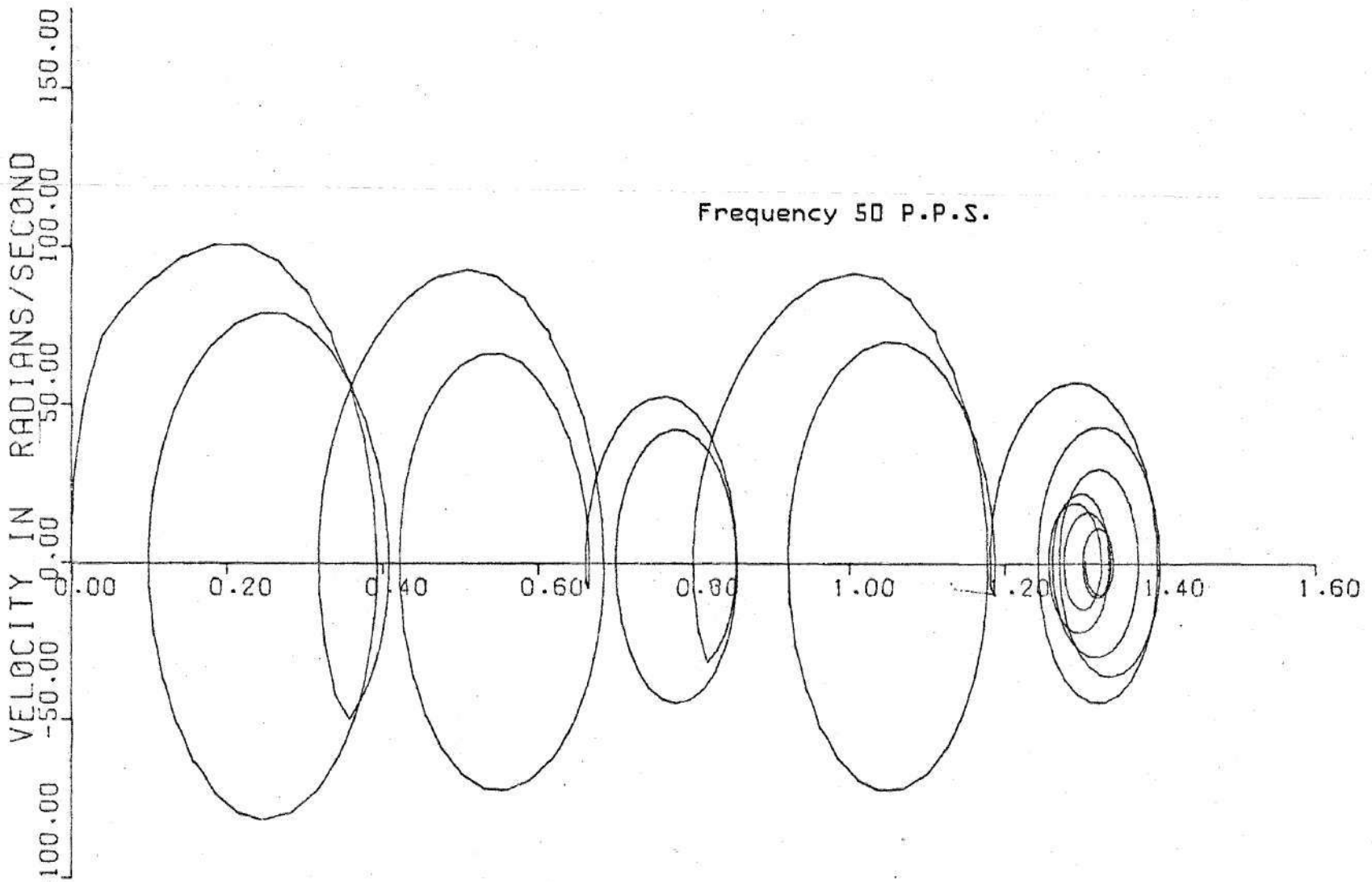

Figure 31. Rotor M.S. State Response

BIBLIOGRAPHY

LITERATURE CITED

(1) R. Bruce Kieburtz, "The Step Motor--The Next Advance in Control Systems," IEEE Transactions on Automatic Control, vol. AC-9, no. 1, January 1964, pp. 98-104.

(2) Ibid.

(3) David J. Robinson, "Dynamic Analysis of Permanent Magnet Stepping Motors," NASA Technical Note N69-20780.

(4) John P. O'Donahue, "Transfer Function for a Stepper Motor," Control Engineering, vol. 8, no. 11, Nov. 1961, pp. 103-104.

(5) Sheldon S. Chang, "An Analysis of the Stepping Motor--What Can It Do?" Proceedings of 1968 NEC, pp. 36-41.

(6) Benjamin C. Kuo, "Modeling and Simulation of a Stepping Motor," IEEE Transactions on Automatic Control, Dec. 1969, pp. 745-747.

(7) David G. Moursund and Charles S. Duris, Elementary Theory and Application of Numerical Analysis. McGraw-Hill Book Co., 1967.

(8) J. J. Stoker, Nonlinear Vibrations. Interscience Publishers 1958.

(9) Op. Cit., Robinson, p. 23.

(10) Donald T. Greenwood, Principles of Dynamics. Prentice-Hall, 1965.

(11) Irving H. Shames, Engineering Mechanics: Statics, Prentice-Hall, 1966.

(12) Arthur E. Snowdon and Elmer W. Madsen, "Characteristics of a Synchronous Inductor Motor," AIEE Transactions on Applications and Industry, vol. 81, Mar. 1962, pp. 1-5.

(13) Francis S. Tse, Ivan E. Morse, and Rolland T. Hinkle, Mechanical Vibrations. Allyn and Bacon Inc. 1966.

OTHER REFERENCES

Bailey, S. J. Incremental Servos. "Part I--Stepping vs Stepless Control." Control Engineering vol. 7, no. 11, Nov. 1960, pp. 123-127; Part II--"Operation and Analysis," vol. 7, no. 12, Dec. 1960, pp. 97-102; Part III--"How They've Been Used," vol. 8, no. 1, Jan. 1961, pp. 85-88; Part IV--"Today's Hardware," vol. 8, no. 3, Mar. 1961, pp. 133-135; Part V--"Interlocking Steppers," vol. 8, no. 5, May 1961, pp. 116-119.

Dunlap, Sam. "Stepping Motor Phase Plane Analysis," Graduate Report Courtesy of Dr. Jay Schlag Georgia Institute of Technology.

Conrad, C. W. "Tormax--Step Servo in Action," Courtesy of IMC Magnetics Corporation.

Fredriksen, T. R. "Stepping Motors Come of Age," Electro-Technology, November 1967, pp. 36-41.

Nicklas, J. C. "Analysis, Design, and Testing of a Position Servo Utilizing a Stepper Motor," ASME Journal of Basic Engineering, June 1963, pp. 211-216.

Wirth, R. L., Filsinger, D. E., and Baumgarten, Jr. "Dynamic Response of a Step Motor" Report No. PEO-1271, Product Engineering Consulting Services, The National Cash Register Company, Dayton, Ohio 45409, June 29, 1965.